

**T
F
A**

**ACTA
FACULTATIS
TECHNICAE**



TECHNICAL UNIVERSITY IN ZVOLEN

1

**ISSUE: XXVIII
ZVOLEN 2023**

Medzinárodný zbor recenzentov / International Reviewers Board

Witold Bialy (PL)

Silesian University of Technology, Faculty of Organization and Management

Igor Ďukič (HR)

University of Zagreb, Faculty of Forestry

Jiří Dvořák (CZ)

Czech University of Life Sciences Prague, Faculty of Forestry and Wood Sciences

Ladislav Dzurenda (SK)

Technical University in Zvolen, Faculty of Wood Sciences and Technology

Roman Gálik (SK)

Slovak University of Agriculture in Nitra, Faculty of Engineering

Zhivko Gochev (BG)

University of Forestry, Faculty of Forest Industry

Radek Knoflíček (CZ)

Brno University of Technology, Faculty of Mechanical Engineering)

Zdeněk Kopecký (CZ)

Mendel University in Brno, Faculty of Forestry and Wood Technology

Ján Kosiba (SK)

Slovak University of Agriculture in Nitra, Faculty of Engineering

Dražan Kozak (HR)

Josip Juraj Strossmayer University of Osijek, Mechanical Engineering Faculty

Antonín Kříž (CZ)

University of West Bohemia, Faculty of Mechanical Engineering

Stanisław Legutko (PL)

Poznan University of Technology

Oleg Machuga (UA)

National Forestry University of Ukraine, Lviv

Milan Malcho (SK)

University of Zilina, The Faculty of Mechanical Engineering

Stanislav Marchevský (SK)

Technical University of Košice, Faculty of Electrical Engineering and Informatics

Ján Mihalík (SK)

Technical University of Košice, Faculty of Electrical Engineering and Informatics

Miroslav Müller (CZ)

Czech University of Life Sciences Prague, Faculty of Engineering

Nataša Náprstková (CZ)

UJEP in Ústí nad Labem, Faculty of Production Technology and Management

Jindřich Neruda (CZ)

Mendel University in Brno, Faculty of Forestry and Wood Technology

Alena Očkajová (SK)

Matej Bel University, Faculty of Natural Sciences

Marián Peciar (SK)

Slovak University of Technology in Bratislava, Faculty of Mechanical Engineering

Krzysztof Zbigniew Rokosz (PL)

Koszalin University of Technology, Faculty of Mechanical Engineering

Juraj Ružbarský (SK)

Technical University of Košice, Faculty of Manufacturing Technologies

Ruslan Safin (RU)

Kazan National Research Technological University

Sergey Spiridonov (RU)

State Institution of Higher Professional Education, Saint Petersburg State

Dana Stančková (SK)

University of Žilina, Faculty of Mechanical Engineering

Vladimír Štollmann (SK)

Technical University in Zvolen, Faculty of Forestry

Marian Šušniar (HR)

University of Zagreb, Faculty of Forestry

Paweł Tylek (PL)

University of Agriculture in Krakow, Faculty of Forestry

Valery Zhylinski (BY)

Belarusian State Technological University

TABLE OF CONTENTS

SCIENTIFIC PAPERS

DETERMINATION OF THE EQUIVALENT STRESSES ON THE TOOTH ROOT OF A HELICAL GEAR PAIR BY MANUAL AND COMPUTATIONAL WAY STANOVENIE EKVIVALENTNÉHO NAPÄTIA NA PÄTE ZUBU HELICKÉHO PREVODU MANUÁLNYM A VÝPOČTOVÝM SPÔSOBOM Sándor Bodzás, Zsolt Tiba	9
EFFECT OF SPINDLE ROTATIONS AND FEED SPEED ON ENERGY CONSUMPTION OF MDF AND PARTICLEBOARDS MILLING ON A CNC MACHINING CENTER VPLYV OTÁČOK A POSUVNEJ RÝCHLOSTI NA ENERGETICKÚ NÁROČNOSŤ FRÉZOVANIA MDF A DTD MATERIÁLOV NA CNC OBRÁBACOM CENTRE Tomáš Čuchor, Peter Koleda, Richard Kminiak	21
APPLICATION OF CONVOLUTIONAL NEURAL NETWORK FOR AUTOMATIC CONTROL OF EDGE BANDING APLIKÁCIA KONVOLUČNEJ NEURÓNOVEJ SIETE NA AUTOMATICKÉ RIADENIE OLEMOVANIA HRÁN Bronislav Dřímal, Jana Procházková	35

SCIENTIFIC PAPERS

DETERMINATION OF THE EQUIVALENT STRESSES ON THE TOOTH ROOT OF A HELICAL GEAR PAIR BY MANUAL AND COMPUTATIONAL WAY

STANOVENIE EKVIVALENTNÉHO NAPÄTIA NA PÄTE ZUBU HELICKÉHO PREVODU MANUÁLNYM A VÝPOČTOVÝM SPÔSOBOM

Sándor Bodzás¹, Zsolt Tiba²

¹ Ph.D., Department of Mechanical Engineering, University of Debrecen, Debrecen, 4028, Hungary

² Ph.D., Department of Department of Air- and Load Vehicle, University of Debrecen, 4028, Hungary

ABSTRACT: A helical gear pair was designed that will be built into a gear box of a vehicle. The geometric design was made by MATLAB software. The computer aided design (CAD) was generated into the SolidWorks software. The assembly and the connection analysis were also made in this software. During the function of the gear pair the determination of the equivalent stress is important to inspect the pinion and the gear for tooth break. The selection of the appropriate material is also mandatory that can bear the prescribed load without tooth break. Considering the recommendation of the references the equivalent stresses were calculated for the pinion and the gear on the two sides of the tooth root. Finite element analysis was made due to the inspection of the correctness of the manual calculation process.

Keywords: helical gear, stress, CAD, FEM

ABSTRAKT: V článku je navrhnutý špirálový ozubený pár, ktorý bude zabudovaný do prevodovky vozidla. Geometrický návrh bol vytvorený softvérom MATLAB. Počítačom podporovaný návrh (CAD) bol realizovaný pomocou softvéru SolidWorks. V tomto softvéri bola vytvorená aj zostava a analýza spojov. Pres právnú funkciu páru ozubených kolies je dôležité určiť ekvivalentné napätie, aby sa skontroloval pastorok a ozubené koleso na zlomenie zubov. Povinný je aj výber vhodného materiálu, ktorý znesie predpísané zaťaženie bez zlomenia zubov. Vzhľadom na odporúčanie z referencií sa vypočítalo ekvivalentné napätia pre pastorok a ozubené koleso na dvoch stranách päty zuba. Z dôvodu kontroly správnosti procesu manuálneho výpočtu bola realizovaná analýza metódou konečných prvkov.

Kľúčové slová: helický prevod, napätie, CAD, FEM

INTRODUCTION

Helical gears are one type of cylindrical gears with slanted tooth trace. Compared to spur gears, they have the larger contact ratio and excel in quietness and less vibration and able to transmit large force. A pair of helical gears has the same helix angle but the helix hand is opposite. Helical gears are often used in automotive transmissions by replacing spur gears (khkgears.net).

The teeth of a helical gear are set at an angle (relative to axis of the gear) and take the shape of a helix. This allows the teeth to mesh gradually, starting as point contact and developing into line contact as engagement progresses. One of the most noticeable benefits of helical gears over spur gears is less noise, especially at medium- to high-speeds. Also, with helical gears, multiple teeth are always in mesh, which means less load on each individual tooth. This results in a smoother transition of forces from one tooth to the next, so that vibrations, shock loads, and wear are reduced (motioncontroltips.com).

We know that a stress state can be comprehensively described by a 3x3 tensor. There is a way that we can use one value to represent the state of a material. Equivalent stress is defined to serve this purpose. In evaluation of stress results, we need 9 contour plots to visualize stress tensor. Equivalent stress allows one to view stress of the structure by one plot. Equivalent stress can be used as a scalar indicator to determine material failure (Equivalent stress, von Misses, stress).

One tooth of a helical gear is considered as a lowing holder that is loaded a perpendicular directional F_N force for the edge of the top land. The friction force is disregarded in this calculation (Terplán, 1975; Litvin et al. 2004).

Supposing planer stress status and using of elementary mechanical method the stress status could be determinable on the tooth root. As a consequence of the load force (F_N) the loads on the tooth roots are pressure (σ_p), bending (σ_b) and shear (τ_s). Based on experiences the highest stresses are received on the G and H points of the tooth root. Based on the references those points can be received by the tangent lines of the fillet radiuses that are angled by 30° in comparison with the symmetric line of the tooth [4]. The G and H points are contact points. The received stresses are based on Figure 1 on the G and H points (Terplán, 1975):

$$\sigma_G = \sigma_{b1} - \sigma_{b2} - \sigma_p \quad (1)$$

$$-\sigma_H = \sigma_{b1} - \sigma_{b2} + \sigma_p \quad (2)$$

Figure 1 shows when only one tooth pair is connected. The stress on the tooth root is the highest if the F_N force effects on the edge of the top land. The stress components can be calculated by the following formulas (Terplán, 1975):

$$\sigma_{b1} = \frac{6 \cdot l_1 \cdot F_N \cdot \cos \alpha_f}{b \cdot v_a^2} \quad (3)$$

$$\sigma_{b2} = \frac{6 \cdot l_2 \cdot F_N \cdot \sin \alpha_f}{b \cdot v_a^2} \quad (4)$$

$$\sigma_p = \frac{F_N \cdot \sin \alpha_f}{b \cdot v_a} \quad (5)$$

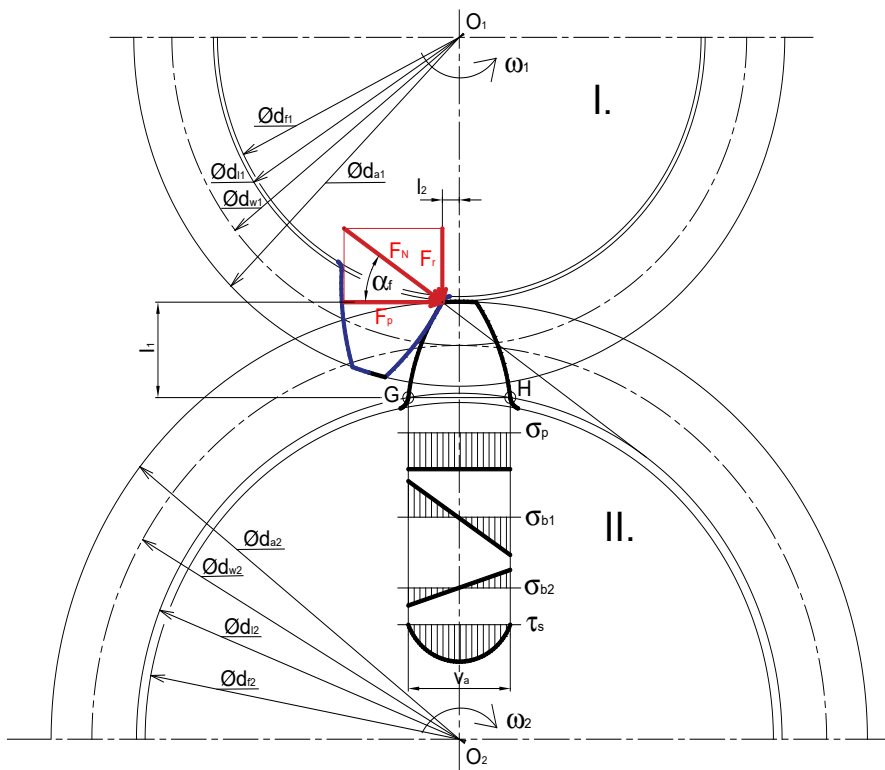


Fig. 1. The stress distribution by the load force
Obr. 1 Rozloženie napätí od záťažovacej sily

Tensile stress is received on the G point. Pressure stress is received on the H point. The Yield limit ($R_{p0.2}$) has to be higher than the s_G and the s_H stresses.

METHOD AND MATERIAL

Geometric design and cad modelling of the helical gear pair

The initial geometric parameters of the helical gear drive can be seen on Table 1.

Considering the initial parameters the output parameters were calculated by a Matlab software where an own-developed program was used. This program can be worked by the

design recommendations of the references (Terplán, 1975 Litvin et al. 2004; Radzevich 2021).

After the geometric design the CAD models of the elements were generated in the SolidWorks software (Figure 2). The assembly and the connection analysis were also made in this software.

Table 1. Initial geometric parameters

Tabuľka 1 Počiatočné geometrické parametre

Number of teeth on the pinion (z_1)	21
Number of teeth on the gear (z_2)	41
Axial module (m_{ax}) [mm]	2.5
Centre distance (a_w) [mm]	91.028
Tool trace (β) [$^\circ$]	30
Face width (b) [mm]	30
Basic profile angle (α_p) [$^\circ$]	20
Connection angle (α_w) [$^\circ$]	25
Number of revolution on the pinion (n) [1/min]	118.3
Loaded moment on the pinion (M_p) [Nm]	262
Type of the material	Strenx P700
Yield limit ($R_{p0.2}$) [MPa]	700
Ultimate strength (R_m) [MPa]	940

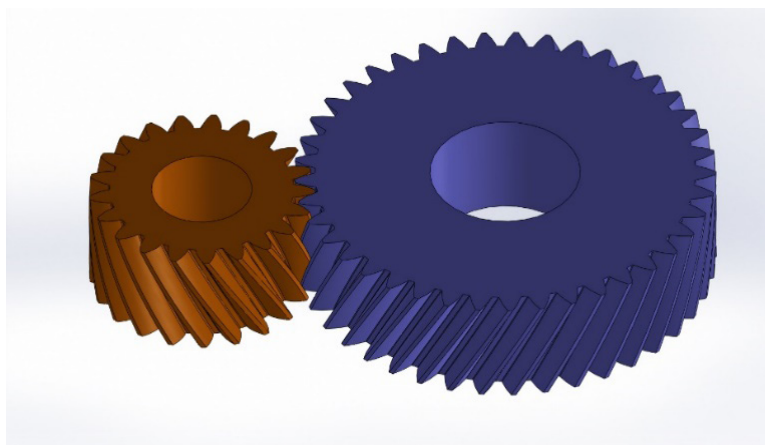


Fig. 2. The CAD assembly of the connecting gear pairs
Obr. 2 CAD zostava spojenia prevodovej dvojice

Knowing of the $d_{a1,2}$ outside diameters the $F_{p1,2}$ perimetric forces can be calculated (Terplán, 1975):

$$F_{p1,2} = \frac{2 \cdot M_{pinion,gear}}{d_{a1,2}} \quad (6)$$

Pinion	$F_{p1} = 7778.381 \text{ N}$
Gear	$F_{p2} = 8111.853 \text{ N}$

Knowing of the $d_{gl,2}$ rolling circle diameters the $\alpha_{f1,2}$ angle is between the perimetric force and the load force (Terplán, 1975)

$$\cos \alpha_{f1,2} = \frac{d_{a1,2}}{d_{g1,2}} \rightarrow \alpha_{f1,2} \quad (7)$$

Pinion	$\alpha_{f1} = 26.96^\circ$
Gear	$\alpha_{f2} = 19.207^\circ$

The $F_{N1,2}$ load forces (Terplán, 1975) are

$$F_{N1,2} = \frac{F_{p1,2}}{\cos \alpha_{f1,2}} \quad (8)$$

The $\sigma_{b11,2}$ bending stresses can be calculated based on (3) formula

Pinion	$F_{N1} = 8726.778 \text{ N}$
Gear	$F_{N2} = 8590.005 \text{ N}$

The $\sigma_{b21,2}$ bending stresses can be calculated based on (4) formula

Pinion	$\sigma_{b11} = 272.809 \text{ MPa}$
Gear	$\sigma_{b12} = 239.441 \text{ MPa}$

The $\sigma_{p1,2}$ pressure stresses can be calculated based on (5) formula

Pinion	$\sigma_{b21} = 272.809 \text{ MPa}$
Gear	$\sigma_{b22} = 239.441 \text{ MPa}$

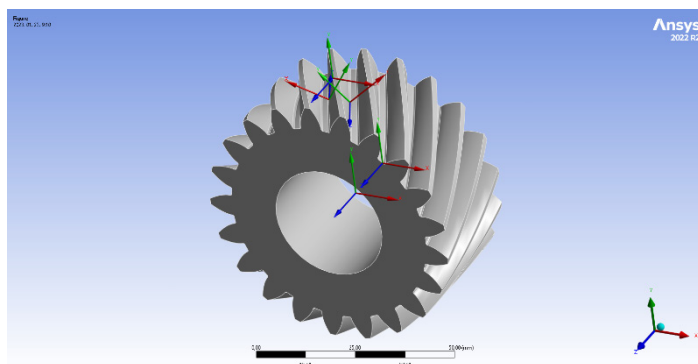
The $s_{G1,2}$ equivalent stresses can be calculated based on (1) formula

Pinion	$\sigma_{p1} = 3.893 \text{ MPa}$
Gear	$\sigma_{p2} = 2.264 \text{ MPa}$

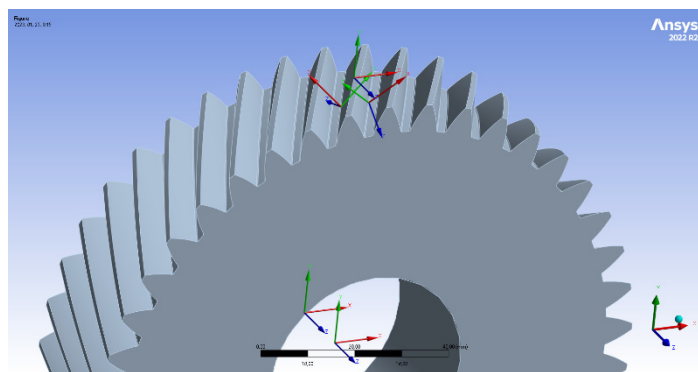
The $s_{H1,2}$ equivalent stresses can be calculated based on (2) formula

Pinion	$\sigma_{G1} = 270.461 \text{ MPa}$
Gear	$\sigma_{G2} = 227.532 \text{ MPa}$

Finite element method analysis

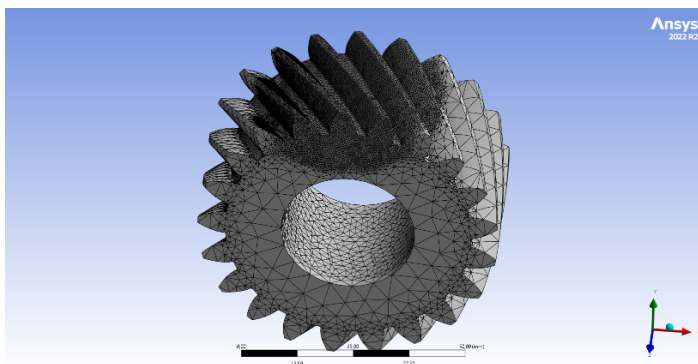


a)

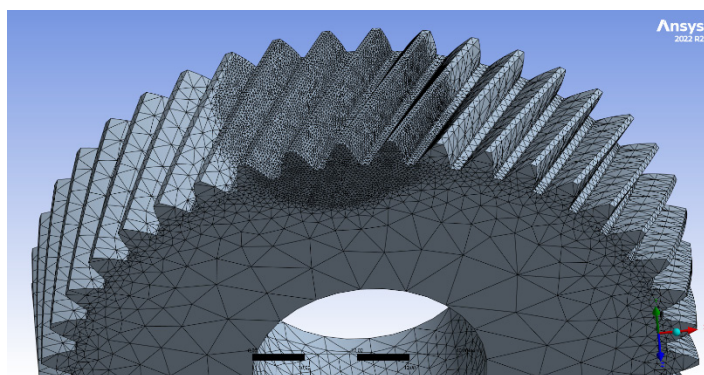


b)

Fig. 3. Adoption of the coordinate systems: a) pinion, b) gear
Obr. 3 Priradenie koordinačných systémov: a) pastorok, b) ozubené koleso

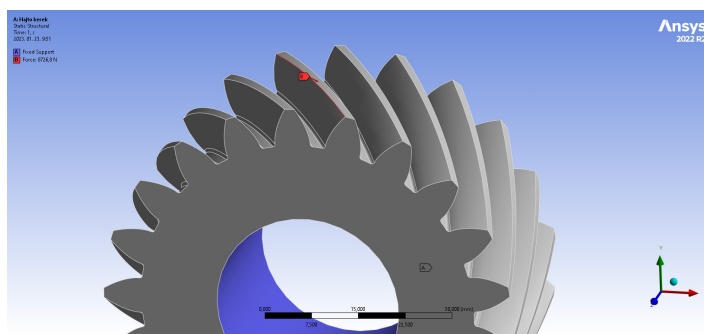


a)

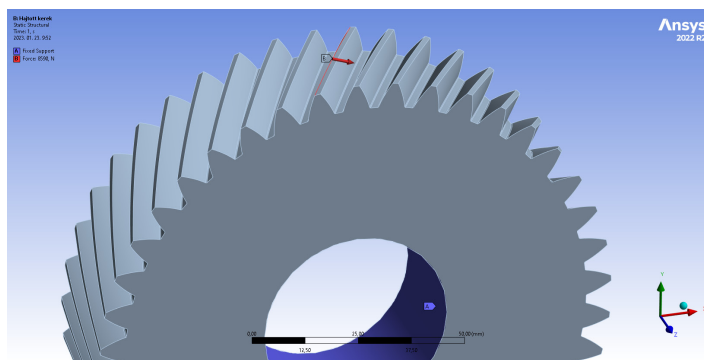


b)

Fig. 4. Adoption of the finite element mesh: a) pinion, b) gear
Obr. 4 Rozloženie meshovacej siete: a) pastorok, b) ozubené koleso



a)

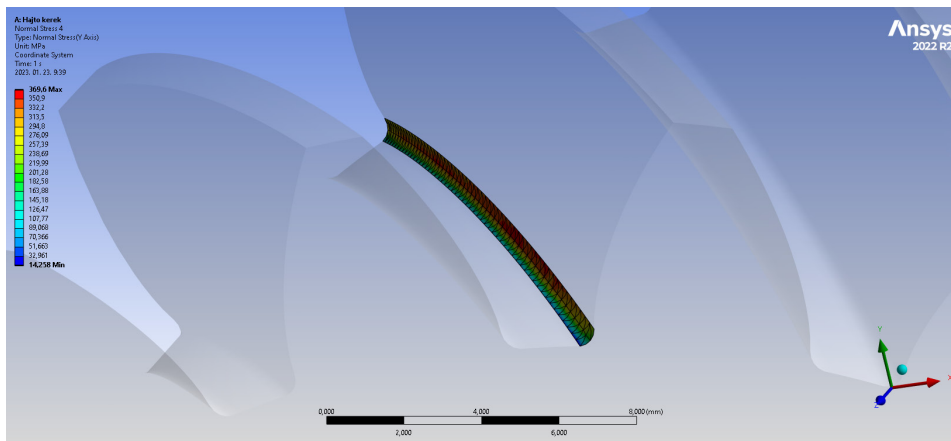


b)

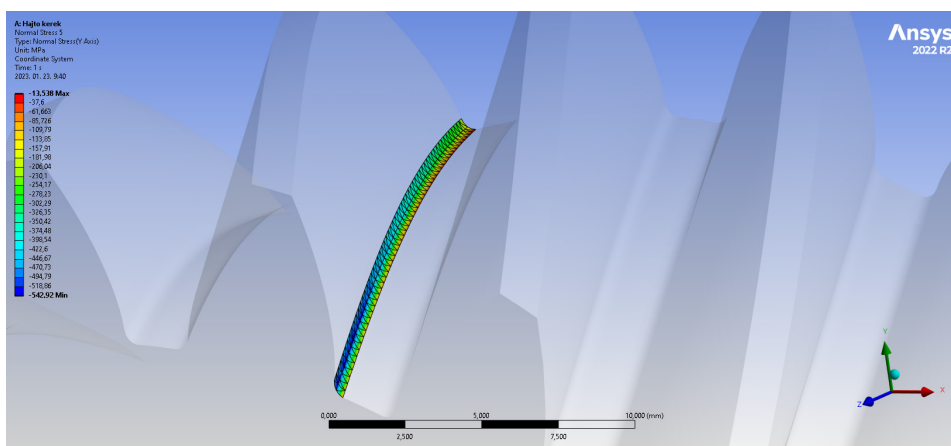
Fig. 5. The adjustment of the load and boundary conditions: a) pinion, b) gear
Obr. 5 Nastavenie zaťaženia a okrajových podmienok: a) pastorok, b) ozubené koleso

Static analysis were done for the pinion and the gear. Coordination systems were adapted on the center line of the gear, the fillet radiuses on the tooth roots and the edge of the top land (Figure 3).

Body sizing was applied for meshing. The meshing density was increased around the zone of the selected tooth where the mesh size is 0.5 mm. Automatic meshing was used on the outside zones (Figure 4).



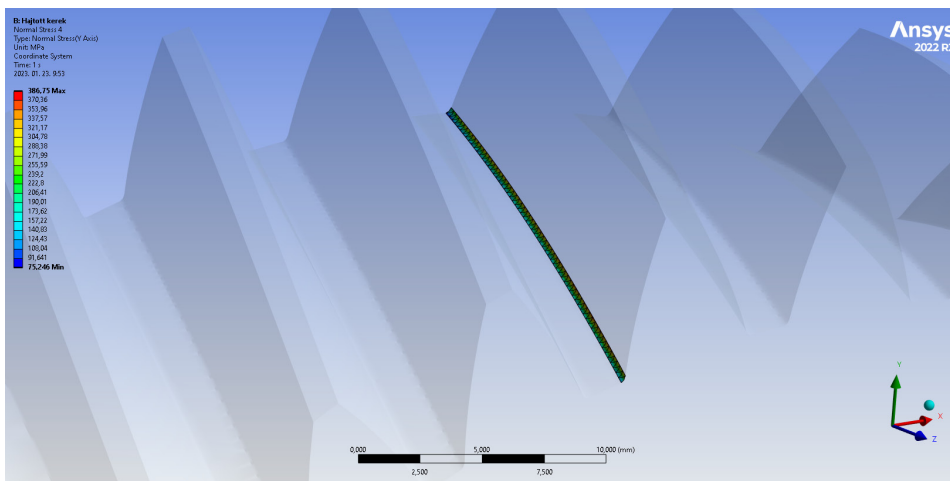
a) G point on the tooth root (the average stress is $\sigma_{G1} = 260.25 \text{ MPa}$)



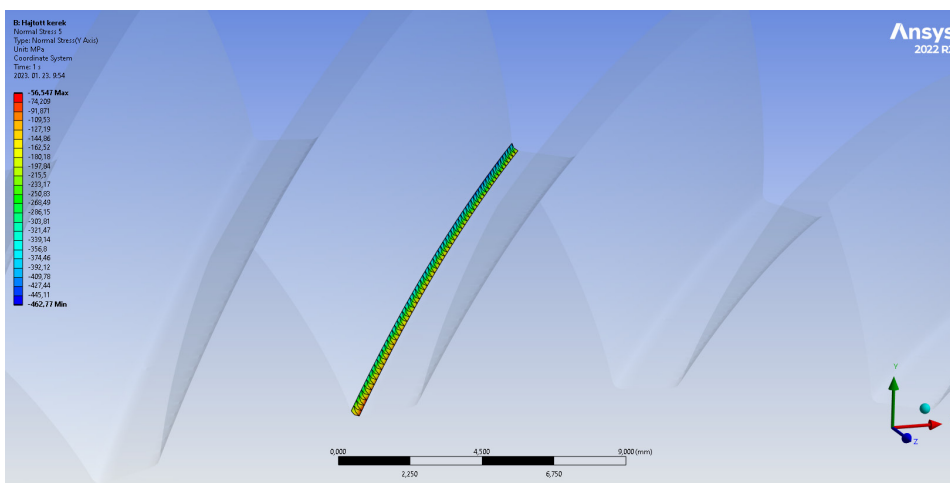
b) H point on the tooth root (the average stress is $\sigma_{H1} = -266.48 \text{ MPa}$)

Fig. 6. Adoption of the finite element mesh on the pinion

Obr. 6 Rozloženie prvkov meshovacej siete na pastorku



a) G point on the tooth root (the average stress is $\sigma_{G2} = 221.312 \text{ MPa}$)



b) H point on the tooth root (the average stress is $\sigma_{H2} = -225.152 \text{ MPa}$)

Fig. 7. Adoption of the finite element mesh on the gear
Obr. 7 Rozloženie prvkov meshovacej siete na ozubenom kolese

The load and boundary conditions can be seen on Figure 5. The calculated force components (8) and (10) were adjusted as loads on the edges of the top lands. After the finite element calculation, the results can be seen on Figure 6 and 7.

RESULTS AND DISCUSSION

Comparing the manual and the computerized calculated results we almost got the same results (Table 2). The reason of the diversions is the applied meshing size. The more the meshing size, the more accurate the finite element results. The applied computer capacity can limit the resolution of the meshing.

Table 2. Comparison of the manual and the computerized results
Tabuľka 2 Porovnanie výsledkov manuálneho a počítačového výpočtu

Equivalent stresses	Type of the gear	Manual results	Computerized results	Deviation
G point	Pinion	$\sigma_{G1}=270.461 \text{ MPa}$	$\sigma_{G1}=260.25 \text{ MPa}$	10.211 MPa
	Gear	$\sigma_{G2}=227.532 \text{ MPa}$	$\sigma_{G2}=221.312 \text{ MPa}$	6.22 MPa
H point	Pinion	$\sigma_{H1}=258.247 \text{ MPa}$	$\sigma_{H1}=266.48 \text{ MPa}$	8.233 MPa
	Gear	$\sigma_{H2}=232.06 \text{ MPa}$	$\sigma_{H2}=225.152 \text{ MPa}$	6.908 MPa

Considering the permissible Yield limit (Table 1) the calculated results are below this limit so the selected material can bear this load that is received by the function of the gear pair.

CONCLUSION

Based on the requirement of the gear box of a vehicle we had to design a helical gear pair. The applied moment and the initial gear parameters were given.

The determination of the gear parameters that are needed for the CAD modelling and the manufacturing are calculated by the Matlab software.

Saving the profile points of the tooth sides interpolation B-spline curves were inserted for the points to get the profile curves. After that the CAD models could be generated into the SolidWorks software.

Determining the equivalent stresses the tooth roots are critical zones of the teeth. The applied force components could be determined from the moments and the transmission ratio.

The equivalent stresses were determined by manual way and computerized way to justify the correctness of the two calculation processes. The computerized calculation was made by the Ansys finite element software.

Comparing the two results of the two ways we diagnose that those results are approximately the same. The difference between them is little where the reason is the meshing strategy that is influenced by the capacity of the applied computer.

ACKNOWLEDGMENT

Project no. **TKP2020-NKA-04** has been implemented with the support provided from the National Research, Development and Innovation Fund of Hungary, financed under the 2020-4.1.1-TKP2020 funding scheme.

REFERENCES

- Equivalent Stress, Von Mises Stress, Solid Mechanics I – Understanding the Physics, Ansys, https://courses.ansys.com/wp-content/uploads/2019/04/1.3.4-Equivalent_-Stress_-rebranded.pdf
- LITVIN, F. L., FUENTES, A. 2004. Gear Geometry and Applied Theory, *Cambridge University Press*, 2004., ISBN 978 0 521 81517 8
- RADZEVICH, S. P. 2021 Dudley's Handbook of Practical Gear Design and Manufacture, Third edition, *CRC Press*, p. 656, ISBN 9781498753104
- TERPLÁN, Z. 1975. Gépelemek IV., Kézirat, *Tankönyvkiadó*, Budapest
- https://khkgears.net/new/helical_gears.html
- <https://www.motioncontroltips.com/helical-gears-what-are-they-and-where-are-they-used/>

Corresponding author:

Name: Dr. **Sándor Bodzás**

Telephone number: +36 70 600 2846

E-mail: bodzassandor@eng.unideb.hu

EFFECT OF SPINDLE ROTATIONS AND FEED SPEED ON ENERGY CONSUMPTION OF MDF AND PARTICLEBOARDS MILLING ON A CNC MACHINING CENTER

VPLYV OTÁČOK A POSUVNEJ RÝCHLOSTI NA ENERGETICKÚ NÁROČNOSŤ FRÉZOVANIA MDF A DTD MATERIÁLOV NA CNC OBRÁBACOM CENTRE

Tomáš Čuchor¹, Peter Koleda¹, Richard Kminiak²

¹*Department of Manufacturing and Automation Technology, Faculty of Technology, Technical university in Zvolen, T. G. Masaryka 24, 960 01, Zvolen, Slovakia,*

²*Department of Woodworking, Faculty of Wood Sciences and Technology, Technical university in Zvolen, T. G. Masaryka 24, 960 01, Zvolen, Slovakia,*

ABSTRACT: The article is devoted to an overview of measurements and evaluation of the energy demand of the machining process with practical implementation in consumption measurements during milling. During the milling process on a CNC machining center, two types of wood-based are processed: MDF and particleboards. The energy demand of the changed technical-technological parameters was tested on experimental samples. The input parameters are the revolutions of the cutter (14 000, 16000 and 18 000 rpm), the feed speed (6, 8 and 10 m.min⁻¹) and the type of material. Subsequently, the electricity consumption of the machining center during the milling process was statistically evaluated. From the investigated technical-technological parameters, the revolutions of cutter have the most statistically significant effect on electricity consumption and thus have the most energetic impact on the production process, followed by feed speed and milled material.

Key words: energy consumption, milling, CNC machining center, electricity consumption, statistical evaluation.

ABSTRAKT: Článok je venovaný prehľadu meraní a vyhodnotení energetickej náročnosti procesu obrábania s praktickou realizáciou pri meraní spotreby počas frézovania. Počas procesu frézovania na CNC obrábacom centre boli opracovávané dva druhy materiálov na báze dreva: MDF a dre-votrieskové dosky. Na experimentálnych vzorkách sa testovala energetická náročnosť technicko-technologických parametrov: otáčky (14 000, 16 000 a 18 000 min⁻¹), posuvná rýchlosť (6, 8 a 10 m.min⁻¹) a druh materiálu. Následne bola štatisticky vyhodnotená spotreba elektrickej energie obrábacieho centra pri procese frézovania. Zo sledovaných technicko-technologických parametrov mali otáčky nástroja najväčší štatistický vplyv na zvýšenie spotreby elektrickej energie a tým najviac energeticky ovplyvňovali výrobný proces, ďalej nasledovala posuvná rýchlosť a druh obrábaného materiálu.

Kľúčové slová: energetická náročnosť, frézovanie, CNC obrábacie centrum, spotreba elektrickej energie, štatistické vyhodnotenie

INTRODUCTION

The manufacturing sector is one of the largest electricity consumers and carbon emitters in the world, accounting for approximately 33% of total energy consumption and 38% of global CO₂ emissions and all associated environmental impacts. On the other hand, rising energy costs also affect the manufacturing industry economically. Reducing the amount of energy consumed and introducing more energy-efficient production processes can significantly increase the performance of processes and reduce their undesirable effects. Machining is one of the most basic and important production processes; new procedures and processes in the production sector are implemented to achieve the main goal of reducing energy consumption. Most of the existing studies on energy reduction in the manufacturing sector focus on the development of the most energy efficient machining processes. The high cost of electricity in the production and processing of materials are among the main factors affecting the final price of products. This is a significant factor underlying the current environmental and economic challenges. While the main goal of scientists in the field of energy efficient production is to achieve minimal energy consumption, they also have the opportunity to look for solutions that are beneficial from an economic and environmental point of view.

In the production process, the energy consumed could be divided into the energy needed to process the material to the required state and the energy consumed by the machine without load. The electrical energy that was consumed by the machine at no load is the energy that is usually consumed by the process unit and its supporting processes. A modern CNC machine tool normally consists of a CNC system, servo control system, feedback communication device, machine bed, lubricant, cooling system, etc. Most machine tools are powered by electricity, where part of the electricity is used to drive the servo systems and the remaining energy is used by the lubrication mechanism, cooling, information display and other auxiliary functions of the machine tool (Figure 1).

1. In the process of machining on the CNC center, electrical energy enters the input.
2. The electrical energy required for the cooling and lubrication system is taken.
3. Power consumption for the power supply module (PSM).
4. Electrical energy consumed by the spindle amplifier module (SPM) for the servo motor driving the spindle.
5. Part of the electrical energy used to drive the spindle motor
6. Energy required for the spindle mechanism.
7. Energy used by the feed axis amplifier module (SVM).
8. Loss of motor energy that enables movement along the sliding axis.
9. Mechanical loss of the servomechanism.

For most servo systems, the AC input is converted to DC through a power supply module (PSM), then the PSM supplies power to the spindle amplifier module (SPM), or the servo axis amplifier module (SVM), respectively, to drive the motor to rotate spindles and turning, or blocking the motor of the feed axis (Liu et al. 2017).

The consumption of critical raw materials (such as steel, aluminium, copper, nickel, zinc, wood, etc. for industrial use has increased worldwide. The rapid growth in manufacturing has created many economic, environmental and social problems from global warming to local waste disposal (Sangwan 2011).

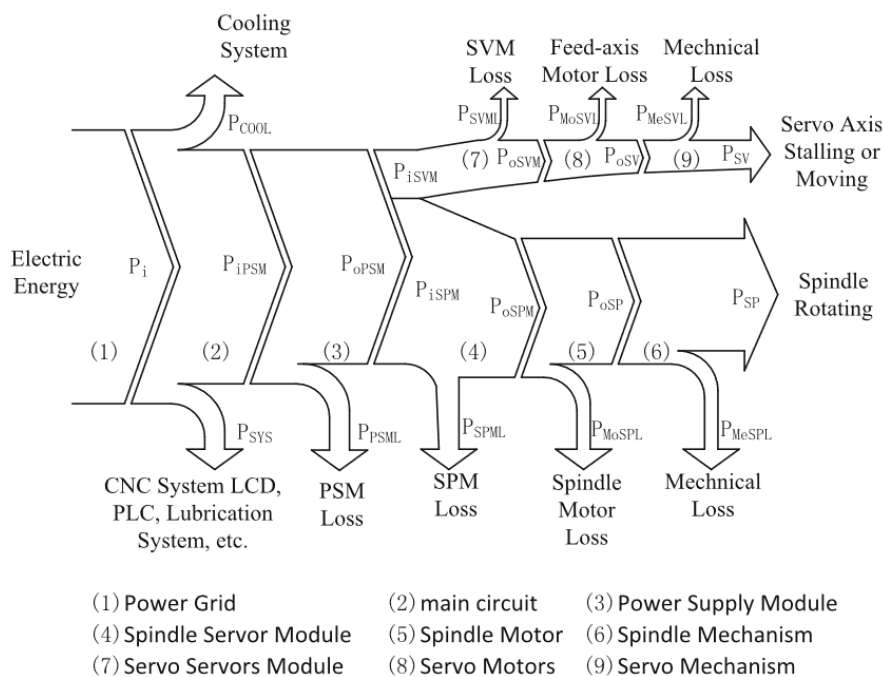


Fig. 1 Energy flow in a CNC production machine (Liu et al. 2017)

Obr. 1 Tok energie v CNC obrábacom centre

Manufacturing processes include a wide range of operations from processes such as machining, grinding and polishing, or injection, pressing, chemical treatment and others. All these production processes take material inputs, including work materials and auxiliary materials, and transform them into products and wastes. Likewise, the energy that enters these processes is transformed into useful work. However, waste heat is a problem. In addition, energy inputs typically require fossil fuels and produce emissions. In the production of electrical energy by burning fossil fuels, this happens in power plants. The flow of the production process together with the material and energy into the process is shown in the figure 1. Energy and its losses. In the production process, a lot of energy is converted into heat. This problem increases our energy costs for the machine. During machining processes, energy loss occurs through the conversion of electrical energy into heat, which is undesirable. This leads to other problems, the increased temperature of the machining tool reduces its service life, increases cooling costs and in some cases leads to malfunctions that slow down or stop production. In an effort to reduce wasted energy in the production process, it is necessary to use the efficiency of the machine. Exergy is a measure of the energy potential of a material that could be converted into energy. By efficient material processing and replacement of machining elements that convert energy into work during the processing process. By increasing their efficiency and eliminating shortcomings, the amount of operating costs can be reduced (Gutowsky et al. 2006).

In order to create techniques to save energy during machining processes and increase energy efficiency, achieving a credible prognostication of energy consumption of machine tools by analysing the power consumption of their various components is essentially required. Using optimized cutting parameters is an effective technique for controlling energy consumption during manufacturing processes (Moradnazhad et al. 2015).

The total power consumption is the addition of air cutting power and material-removal power. Air cutting power is the power required by a machine tool when cutting tool is ready to cut the material from the workpiece without contacting the workpiece and follows the same tool path as during the material removal. The material removal power is the difference between total power and air cutting power. Based on material removal, the machining processes in machine tools can be classified into constant- material removal rate (MRR) and variable-MRR. In the constant-MRR machining process, all the cutting parameters remain unchanged during the machining for example turning and milling whereas, in variable-MRR, at least one of the cutting parameter changes e.g. end face turning, chamfering and grooving etc. (Pawanr et al. 2021).

The machining process of a workpiece actually involves both constant-MRR and variable-MRR machining processes. The energy consumed during variable-MRR machining contributes to a significant portion of the total energy consumption. Thus, to evaluate the total energy consumption during the machining of an actual workpiece, variable-MRR machining energy consumption is also equally important. The development of accurate energy consumption model of machine tools is foundation for the selection of optimal process parameters in a machining process that could lead to sustainable manufacturing during the life cycle of a product (Pawanr et al. 2021).

This article provides a practical example of measuring machine consumption during machining with a subsequent evaluation of the influence of individual technical-technological parameters on this consumption.

MATERIAL AND METHODS

The measurements were realised on an MDF board with dimensions of $500 \times 300 \times 18$ mm and a weight of 1960 g. The experimental samples were sawn from a 2800×2070 mm board. The density of the material was in the range of $720 - 740 \text{ kg}\cdot\text{m}^{-3}$.

The particleboards of the same dimensions have been added as reference samples. The density of particleboard given by the manufacturer was $600 - 640 \text{ kg}\cdot\text{m}^{-3}$. Formaldehyde glue with an admixture of paraffin was used in the production.

Both materials come from Kronospan Ltd. (Zvolen, Slovakia). The manufacturer declared that the material complies with EN 14 322, EN 312-2 and emission class E1 (EN ISO 12460-5) (EN 14322, EN 312-2, EN ISO 12460-5).

The measurement was carried out on the CNC milling center SCM TECH Z5 from the company SCM – group, Rimini, Italy and was carried out in the laboratories of the Technical University in Zvolen.

Table 1 Parameters of the 5-axis CNC machining center SCM TECH Z5
Tabuľka 1 Parametre 5-osého CNC obrábacieho centra SCM TECH Z5

Axes ¹⁾		
Working area along X-Y-Z axes ²⁾	mm	3050 – 1550 – 160
Panel length along Y axis ³⁾	mm	1550
Panel length (for alternated work process) ⁴⁾	mm	1390
Vectorial speed X-Y axes ⁵⁾	m.min ⁻¹	83
Electrospindle ⁶⁾		
Std motor power ⁷⁾	KW (Hp)	11(15)
Max. speed ⁸⁾	rpm	20 000

¹⁾Osi, ²⁾Pracovná oblasť pozdĺž osí X-Y-Z, ³⁾Dĺžka panelu pozdĺž osi Y, ⁴⁾Dĺžka panelu (alternatívny pracovný proces), ⁵⁾Vektorová rýchlosť v osiach X-Y, ⁶⁾Elektrovretno, ⁷⁾Výkon motora, ⁸⁾Maximálne otáčky,

By correctly choosing the technical parameters and geometry of the machining tool, it is possible to save considerable capital. Incorrect geometry of the tool leads to an increase in costs, most often it leads to a reduced lifespan of the machining tool.

During the experimental milling, the tools shown in fig. 2 and 4 with technical parameters in tab. 2 and 3 were used. The dimensions of tools and chips direction are shown in the fig. 3 and 5 for better comprehensibility.

Table 2 Technical parameters of milling tool spiral cutter
Tabuľka 2 Technické parametre frezovania

Tool length ¹⁾	$L = 157,8 \text{ mm}$
Tool diameter ²⁾	$D = 20 \text{ mm}$
Working length of tool ³⁾	$B = 75 \text{ mm}$
Maximum feed ⁴⁾	$f_{\max} = 20 \text{ m.min}^{-1}$
Minimum feed ⁵⁾	$f_{\min} = 6 \text{ m.min}^{-1}$
Maximum speed ⁶⁾	$n_{\max} = 20\,000 \text{ rpm}$
Standard speed ⁷⁾	$n = 18\,000 \text{ rpm}$
Chip direction ⁸⁾	positive

¹⁾Dĺžka nástroja, ²⁾Priemer nástroja, ³⁾Pracovná dĺžka nástroja, ⁴⁾Maximálny posuv, ⁵⁾Minimálny posuv, ⁶⁾Maximálna rýchlosť, ⁷⁾Odporúčaná rýchlosť, ⁸⁾Smer odvodu triesky,



Fig. 2 Roughing tool
Obr. 3 Hrubovací nástroj

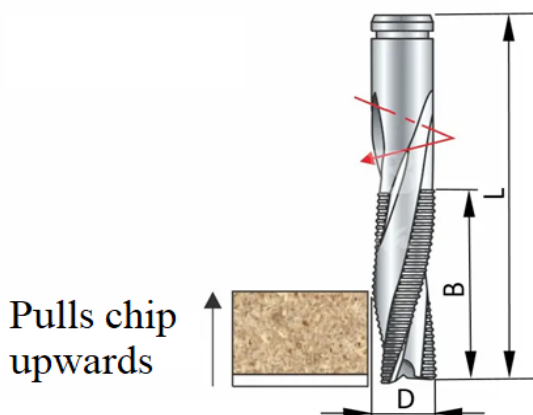


Fig. 3 Diagram of the positive roughing cutter tool, D – tool diameter, B – tool working length, L – tool length (www.freudtools.com)
Obr. 3 Pozitívna hrubovacia fréza, D – priemer nástroja, B - pracovná dĺžka nástroja, L - dĺžka nástroja

Table 3 Technical parameters of finishing tool spiral cutter
Tabuľka 3 Technické parametre dokončovacieho nástroja

Tool length ¹⁾	$L = 213,26 \text{ mm}$
Tool diameter ²⁾	$D = 20 \text{ mm}$
Working length of tool ³⁾	$B = 110 \text{ mm}$
Maximum feed ⁴⁾	$f_{\max} = 20 \text{ m.min}^{-1}$
Minimum feed ⁵⁾	$f_{\min} = 6 \text{ m.min}^{-1}$
Maximum speed ⁶⁾	$n_{\max} = 20\,000 \text{ rpm}$
Standard speed ⁷⁾	$n = 18\,000 \text{ rpm}$
Chip direction ⁸⁾	negative

¹⁾Dĺžka nástroja, ²⁾Priemer nástroja, ³⁾Pracovná dĺžka nástroja, ⁴⁾Maximálny posuv, ⁵⁾Minimálny posuv, ⁶⁾Maximálna rýchlosť, ⁷⁾Odporúčaná rýchlosť, ⁸⁾Smer odvodu triesky,



Fig. 4 Finishing tool
Obr. 4 Dokončovací nástroj

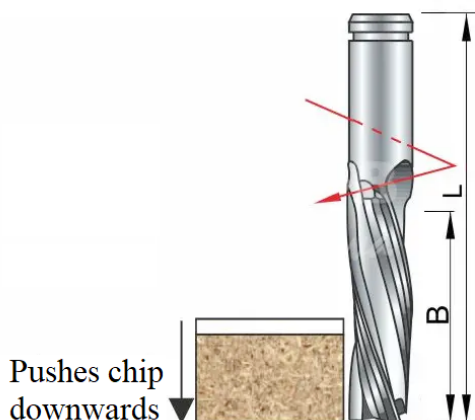


Fig. 5 Diagram of the negative finishing cutter tool, B – tool working length, L – tool length (www.freudtools.com)

Obr. 5 Negatívna dokončovacia fréza, B - pracovná dĺžka nástroja, L - dĺžka nástroja

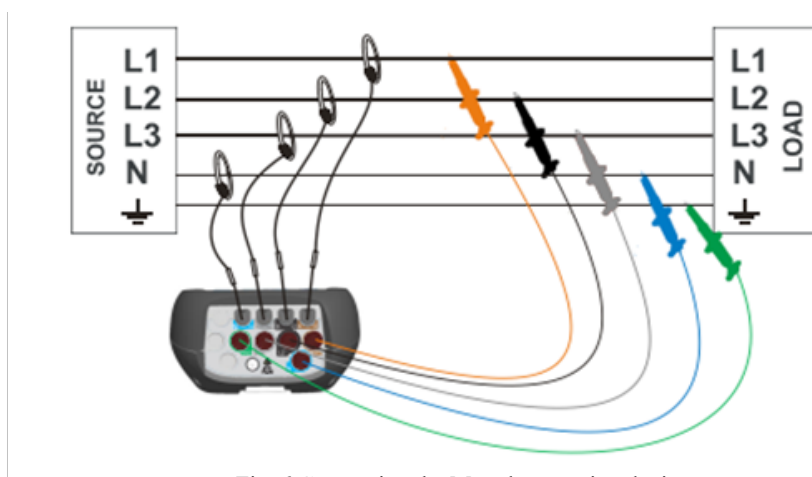


Fig. 6 Connecting the Metrel measuring device
Obr. 6 Zapojenie analyzátora Metrel do elektrickej siete

The power analyser was connected to the electrical power supply of the CNC machining center. It was connected with the help of current probes and voltage clamps. The voltage clamps were connected to the phase conductors, zero and protective conductor using the installed socket 32 A5P. The current probes were connected in the direction of the current flow, in the case of the opposite connection, the values measured on the terminals would be negative. After the connection of measuring circuit, a test measurement of the signal was realized on the phases.

The CNC program was programmed as linear movement from point A to point B. Technological parameters of milling are in tab. 4.

Table 4 Technological parameters of milling
Tabuľka 4 Technologické parametre frézovania

Technological parameters of milling			
Revolutions1) (n) [1000rpm]	14	16	18
Feed2) (f) [m.min-1]	6	8	10

1)Otáčky, 2)Posuv

The measured data had to be processed, to access the measured data the Metrel Power View program was used, which then opened each measurement separately. The measurements contained all the information on the measurement values that the device allowed us to measure. For the purpose of the work, the required data was manually transcribed into Excel. By processing the measured data under milling load and without load, information of the amount of energy consumed during the machining process was found. Subsequent evaluation of effect of rotations, feed speed and milled material on cutting power was realised in the program Statistica.

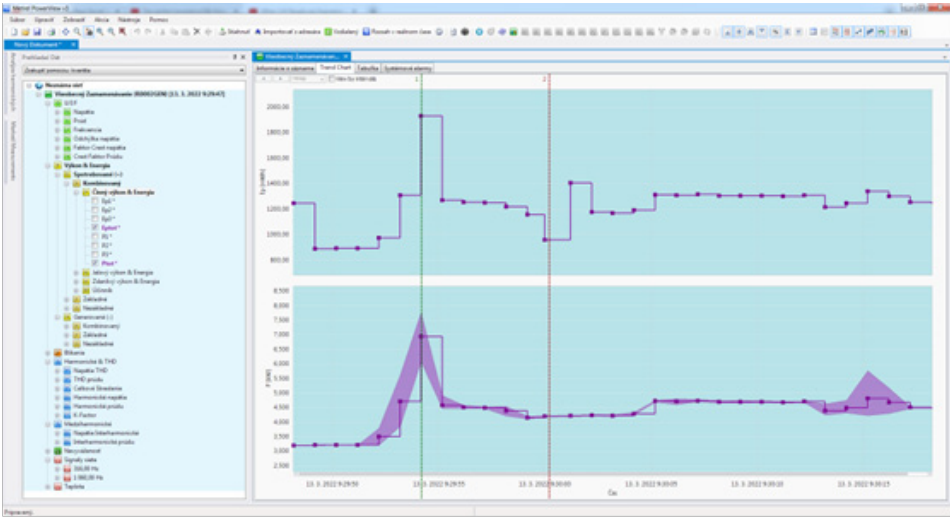


Fig. 7 Program environment Metrel Power View
Obr. 7 Programovacie prostredie Metrel Power View

RESULTS AND DISCUSSION

Description statistics of measured and calculated values of power during milling is described in the table 5.

Table 5 Description statistics of cutting power

Tabuľka 5 Popisná štatistika rezného výkonu

Parameter	Value ¹⁾	Average ²⁾ P [kW]	St. Dev. ³⁾ [kW]	-95,0 % [kW]	+95,0 % [kW]
n [rpm]	14000	3,36	0,23	3,26	3,46
	16000	3,68	0,28	3,56	3,80
	18000	4,07	0,39	3,91	4,24
f [m.min ⁻¹]	6	3,68	0,43	3,50	3,86
	8	3,66	0,44	3,47	3,84
	10	3,78	0,40	3,61	3,95
Material	Particleboard ⁴⁾	3,73	0,45	3,58	3,89
	MDF	3,67	0,40	3,54	3,81

¹⁾Hodnota, ²⁾Priemer, ³⁾Smerodajná odchýlka, ⁴⁾Drevotriesková doska

F-statistic and the corresponding p-value of ANOVA are in the table 6. When analyzing all the combinations, it was found that mainly the revolutions of cutting toll, have a significant influence on the consumption of electricity. It is assumed that the consumption of electrical energy by the feed of the tool will increase if the speed of the cutting tool increases. It was predicted that with increased revolutions of cutting tool the energy consumption rises.

Table 6 Statistical method of ANOVA

Tabuľka 6 Štatistická metóda ANOVA

Effect	One dimensional results for each dependent. variable				
	Degrees of freedom ¹⁾	P [kW] (SS ²⁾)	P [kW] (MS ³⁾)	F ⁴⁾	p ⁵⁾
Abs. member	1	987,56	987,56	17643,48	0,000
Revolutions (n)	2	6,0922	3,0461	54,42	0,000
Feed (f)	2	0,2041	0,1021	1,82	0,176
Material	1	0,0627	0,0627	1,12	0,296
n . f	4	0,0895	0,0224	0,40	0,807
n. Material	2	0,2819	0,1410	2,52	0,094
f. Material	2	0,0525	0,0263	0,47	0,629
n . f. Material	4	0,4376	0,1094	1,95	0,122
Error	36	2,0150	0,0560		
Total	71	12,6241			

SS means "the sum of squares due to the source."

MS means "the mean sum of squares due to the source."

F means "the F-statistic."

P means "the P-value."

¹⁾Stupeň voľnosti, ²⁾Súčet štvorcov, ³⁾Priemerný súčet štvorcov, ⁴⁾Hodnota testovacieho kritéria, ⁵⁾

Hladina významnosti (hypotézu H0 možno zamietnuť, ak $p < 0,05$)

Duncan's test (method of more detailed evaluation) shows a mutual comparison of averages with each other. From the values presented in the table, it can be noted that there is a difference between the speed of rotation of spindle in terms of electricity consumption and they have a statistically significant difference. It can be concluded that with an increase in revolutions, the overall consumption of energy is also increased, that means that this factor has a statistically significant effect. The graphic interpretation is shown in more detail on the speed chart in fig. 8. In the graph, it can be also seen how the consumption of electricity increases linearly with the increase in the speed of the machining tool.

Table 7 Duncan's test for revolutions

Tabuľka 7 Duncanov test pre otáčky

revolutions [1000 rpm]	14 M = 3,360	16 M = 3,679	18 M = 4,072
14		0,000159	0,000063
16	0,000159		0,000122
18	0,000063	0,000122	

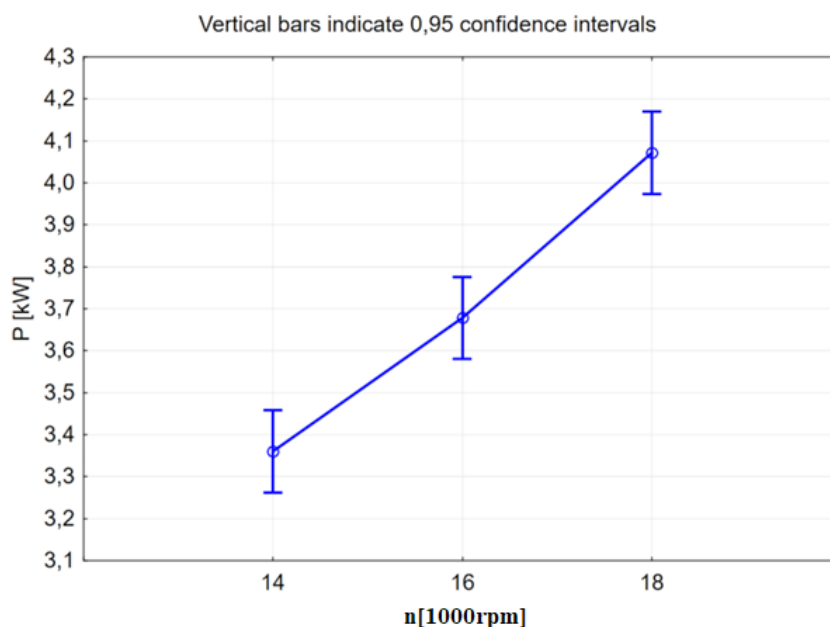


Fig. 8 Dependence of the consumption of electricity on the revolutions of the milling tool

Obr. 8 Závislosť rezného príkonu na otáčkach

On the basis of the experiments carried out and their evaluation through analysis of dispersion followed by post-hoc test, it can be concluded that with increasing revolutions of spindle of machine center, the electrical output also increased almost linearly from value of 3,36 kW and speed of 14 000 rpm to the value of 4,07 at speed of 18 000 rpm.

This increase is caused by the increase in the values of currents flowing through the windings of the electric drive for spindle and also by the increased volume of removed material pre unit of time. The increase in power required to remove material is also confirmed by the authors (Sedlecký et a. 2017) who examined power consumption during edge milling of MDF and edge-glued panel and also (Barčík et a. 2010) who examined the effect of various feed rates and cutting speed on power consumption during the surface milling of beech wood. The change in revolutions had a statistically significant effect on the change in the consumed electrical energy (parameter $p < 0.05$).

With Duncan's test shows a mutual comparison of the averages of electricity consumption by the spindle speed. From the values presented in the table, it can clearly pointed out that the speed of the tool movement of the machining center does not confirm a statistically significant dependence to current consumption of electricity. It can be concluded that the energy consumption is not significantly increased with the acceleration of the movement of machining tool, this factor does not have a statistically significant effect. The graphical interpretation is shown in more detail on the shift graph in fig. 9. From the graph, it can be seen that the largest consumption was precisely when the tool was moved 10 meters to the right. Acceleration of the machining tool will not significantly increase our consumption of electrical energy.

Table 8 Duncan test for feed speed
Tabuľka 8 Duncanov test pre posuv

Feed speed [m.min-1]	6 M = 3,678	8 M = 3,655	10 M = 3,778
6		0,743	0,151
8	0,743		0,097
10	0,151	0,097	

When the feed speed changed from 6 to 8 m.min-1, the cutting power decreased from 3.38 to 3.66 kW, when it changed to 10 m.min-1, it increased to 3.78 kW. Small increase of milling output with increase of feed speed also stated (Sedlecký et a. 2017) and also (Atanasov and Kovatchev 2019) who examined cutting power during milling of wood based materials as MDF and plywood. However, Duncan's post hoc test did not show statistical significance of this change.

Duncan's test can show a mutual comparison of averages between electricity consumption and material. From the values listed in the table, it can be stated with certainty that the type of processed material during milling does not confirm a statistically significant dependence of the consumption of electricity on the consumption in the machining center. It can be also concluded that the DTD material being replaced by the MDF material do not lead to significant energy savings in consumption. Replacing type of woods does not significantly increase the consumption of electricity in the process of machining the material. Graphical interpretation is shown in more detail on the materials chart. From the graph, it can be determined that DTD materials and MDF materials are similar. Visually, the materials did not look different with the naked eye. However, the total electrical energy consumption for paricleboardwas greater than the energy consumption needed to process MDF.

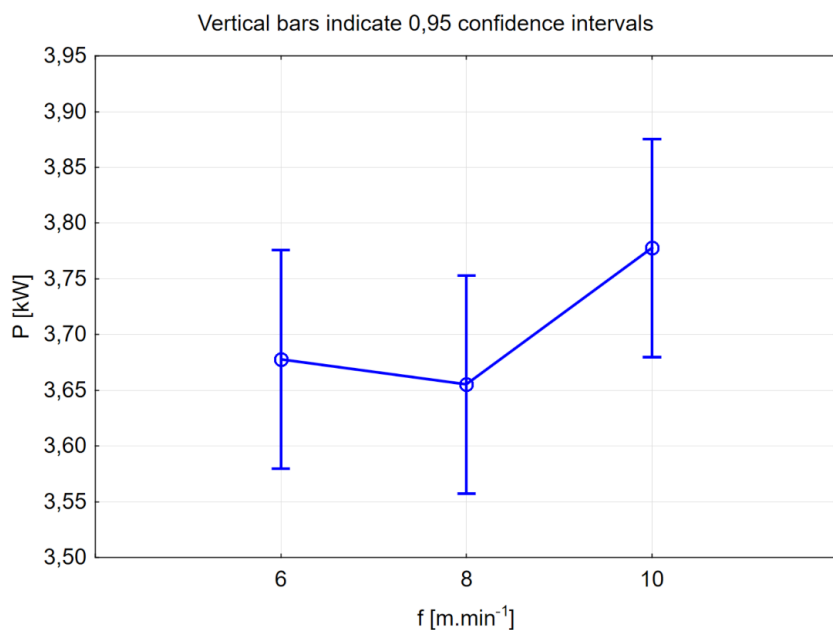


Fig. 9 Dependence of electrical power consumption on feed speed
Obr. 9 Závislosť rezného príkonu na posuvnej rýchlosti

Table 9 Duncan's test of materials

Tabuľka 9 Duncanov test pre materiály

Material	1 Particleboard1) M = 3,733	2 MDF M = 3,674
1 Particleboard1)		0,296
2 MDF	0,296	

¹⁾Drevotriesková doska

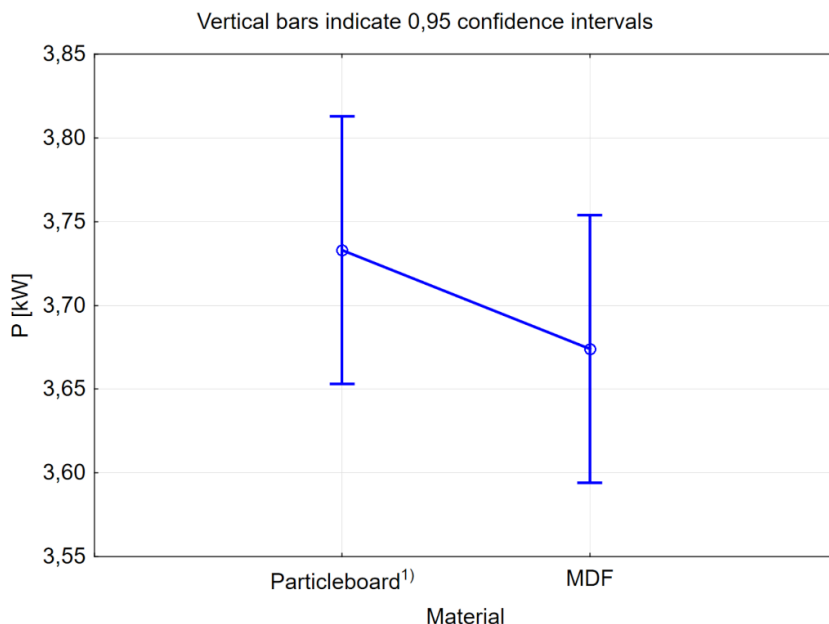


Fig. 10 Dependence of the consumption of the average electrical energy process on milled material

Obr. 10 Závislosť rezného príkonu na frézovanom materiále

Power requirement for machining was higher during milling particleboard (3,73 kW) than medium density particleboards (3,67 kW) despite of that MDF has higher density than particleboard. However, the difference in power consumption between the material was not statistically significant.

CONCLUSION

Reducing the energy demand of not only processes in the manufacturing industry is one of the current challenges of society for sustainable production. This also includes analysing the factors that have the greatest influence on consumption and which are modifiable, while other economic and material parameters must also be taken into account. The results of the experiment confirmed that the greatest influence on the energy consumption of milling are revolutions of the tool, or cutting speed. The effect of milled materials and feed speed did not show statistical significance. These findings will be further expanded and deepened in further research.

ACKNOWLEDGMENT

The research was conducted through project APVV-20-0403: FMA analysis of potential signals suitable for adaptive control of nesting strategies for milling wood-based agglomerates

REFERENCES

- ATANASOV, V., KOVATCHEV, G. 2019. Determination of the cutting power during milling of wood-based materials. *Acta Facultatis Xylogiae*. 61. 93-101. 10.17423/afx.2019.61.1.09.
- BARCÍK, Š., KMINIAK, R., ŘEHÁK, T., KVIETKOVÁ, M. 2010. The influence of selected factors on energy requirements for plain milling of beech wood. *Journal of Forest Science*. 56. 243-250. 10.17221/119/2009-JFS.
- www.freudtools.com page of Freud®. [online] [cit. 2023-10-31]. Available on: <<https://www.freudtools.com/public/catalog/freud-catalog/>>.
- GUTOWSKI T, DAHMUS J, THIRIEZ A 31.05.2006 Electrical Energy Requirements for Manufacturing Processes [online]. [cit. 2023-10-12]. Available on: <<http://web.mit.edu/2.813/www/readings/Gutowski-CIRP.pdf>>
- HORTOBÁGYI, A. 2023. Analýza vibrácií obrobku ako potenciálneho parametra preadaptívne riadenie CNC stroja. PhD-thesis. Zvolen: Technická univerzita vo Zvolene. Fakulta techniky. 2023. 113 s.
- LIU, Z. ZHANG, W., LIU, L., XIAO, Z. 2017 Measuring and calculating the computer numerical control lathe's cutting power and total electric power consumption based on servo parameters [online]. [cit. 2023-10-12]. Available on: <<https://journals.sagepub.com/doi/pdf/10.1177/1687814017723293>>
- MORADNAZHAD M, UNVER H.O. 2015 Energy Efficiency of machining operations: A Review. *Proc IMechE Part B J Engineering Manufacture*, 1–19
- PAWANR, S., GARG, K.G., ROUTROY, S. 2021 Modelling of Variable Energy Consumption for CNC Machine Tools Department of Mechanical Engineering, Birla Institute of Technology and Science, Pilani, Rajasthan, INDIA –333031
- SANGWAN, K. S., 2011. Development of a multi criteria decision model for justification of green manufacturing systems. *Int. J. Green. Econ.* 5, 285-305
- SEDLICKÝ, M., GAŠPARÍK, M. 2017. Power consumption during edge milling of medium-density fiberboard and edge-glued panel. *Bioresources*. 12. 7413-7426. 10.15376/biores.12.4.7413-7426.

Corresponding author:

Tomáš Čuchor, xcuchor@is.tuzvo.sk

APPLICATION OF CONVOLUTIONAL NEURAL NETWORK FOR AUTOMATIC CONTROL OF EDGE BANDING

APLIKÁCIA KONVOLUČNEJ NEURÓNOVEJ SIETE NA AUTOMATICKÉ RIADENIE OLEMOVANIA HRÁN

Bronislav Dřímal¹, Jana Procházková²

¹ Department of Design and Furniture, Faculty of Forestry and Wood Technology, Mendel University, Zemědělská, 616 69, Brno, Czech Republic, bronislavdrimal@email.cz

² Department of Mathematics, Faculty of Mechanical Engineering, Brno University of Technology, Technická 3, 616 69, Brno, Czech Republic, prochazkova.j@fme.vutbr.cz

ABSTRACT: Furniture firms are increasingly seeking to meet Industry 4.0 requirements by incorporating automation in production. Our article addresses the automated inspection of the edge to be banded at the time of the banding process. By using a camera placed above the roller conveyor behind the banding machine, which contains a neural network, we want to automatically detect the type and possible error after the edge banding has been performed. For each image, filtering is performed using Gabor and Canny filters to highlight edges, defects and remove noise. Next, our proposed convolutional neural network evaluates the edge banding quality in real-time and detects the thickness of the edge band for the higher-level system's requirements. For comparison, we created a series of adapted pre-trained neural networks (GoogleNet, ResNet, DarkNet, etc.) and compared them with our suggested neural network concerning precision and computational complexity. This technology expands the current infrastructure for enterprises and is suitable for businesses of any size. Additionally, it offers the benefit of effortless expandability to other varieties of mistakes or banding types.

Key words: banding machine, convolutional neural network, Industry 4.0, quality control, automation, edge AI, oak-d

ABSTRAKT: Nábytkárske firmy stále chcú stále častejšie spĺňať požiadavky konceptu 4.0 zavedením automatizácie do výroby. Naš článok sa zameriava na automatickú kontrolu olepovanej hrany pri procese olepovania. Pomocou kamery umiestnenej nad valčekovým dopravníkom za olepovacím strojom, ktorá obsahuje neurónovú sieť, chceme automaticky detegovať typ a prípadnú chybu po olepení hrany. Pre každý snímok je realizovaná filtrácia pomocou Gabor a Canny filtrov, ktoré zvýraznia hrany, vady a odstránia šum. V ďalšom kroku pomocou nami navrhutej konvolučnej neurónovej siete vyhodnocujeme v reálnom čase kvalitu olepenia a zisťujeme hrúbku olepovanej hrany pre potreby nadradeného systému. Pre porovnanie sme vytvorili sadu upravených predtrénovaných neurónových sietí a nami navrhnutú neurónovú sieť sme s nimi porovnali z hľadiska presnosti a výpočtovej náročnosti. Táto technológia rozširuje aktuálne strojné vybavenie podniku a je vhodná pre firmy všetkých veľkostí. Jej výhodou je tiež jednoduchá rozšíriteľnosť na ďalšie druhy chýb alebo druhy olepenia.

Kľúčové slová: olepovač, konvolučné neurónové siete, filtrovanie obrazu, umelá inteligencia,

INTRODUCTION

The study focuses on automated control and data collection during the banding process on a banding machine. Edge banding is an essential component for furniture manufacturing and protection. Automating the process improves quality control and aligns it with the objectives of Industry 4.0. Primary edge banding activities include applying adhesive, attaching and pressing the edge banding material, curing the adhesive, and removing overlaps. The bonding process is a complex technological procedure used in the treatment of sheet material. This complexity is due to the production equipment which consists of a fluctuating number of units. The main units include pre-milling, taping, dripping, milling, copying and polishing. Alongside these primary units, the machines are equipped with additional units such as flat or profile squeegees and cleaning brushes. Traditional machinery design uses rollers or nozzles to apply EVA or PUR adhesive. Innovative techniques, such as laser, plasma, hot air and SLIM-LINE technology, have also emerged, which apply adhesive to adhesive tapes rather than the part. These technologies are concerned with techniques for adhering tape. After the edge banding process, the component is transported via a conveyor belt to the aggregates, which remove the edge overlap from the base material. This procedure is the same for all machinery, regardless of manufacturer. Our investigation focuses on overseeing the glueing process itself and the resulting aggregates.

The intelligent manufacturing system is the primary system for intelligent machinery, incorporating all production processes within the plant, from machinery and equipment to logistics management. In a smart factory, each part of the semi-finished product is fitted with an electronic tag such as a QR code or RFID (Wang et al. 2017).

The furniture industry faces many challenges in the form of low machine efficiency and high labour costs. Smart manufacturing is becoming an inevitable trend for the future furniture industry. Industry 4.0 focuses on efficient machine allocation, quick response to market demand, low labour costs along with reduction in logistics costs (Wang et al. 2017).

In the case of medium-sized enterprises, it is a frequent practice to substitute small woodworking machines with a nested arrangement of machines consisting of a cutting centre with a disorganised stock, banding centre, milling centres, and CNC machine tools. Every workstation is fitted with automatic part loading and unloading. This method results in a production increase of around 30-40% for manufacturers. It also tackles the shortage of human workers.(Červený et al. 2022).

One objective of Industry 4.0 is the development of smart factories that rely on data and intelligent devices for computation, communication and precision control. In the daily operation of a smart factory, it is crucial that the software controlling the robotic centres, specifically the banding centre in this case, is mature. Usually, workers carry out inspections after each operation, but sometimes these are omitted during the packaging process. In the context of Industry 4.0, wherein robots perform operations rather than humans, it is essential to measure product quality. A review of the literature indicates that this study expands the current knowledge in this field (Wang et al., 2017; Cervený et al., 2022).

Due to specific customer needs and the individualisation of products, manufacturers must constantly broaden the range of materials they produce. In the case of flat materials, this typically refers to the different colour versions. In banding machines, a stack of

banding materials of various sizes is present, providing a ready supply of tens or even hundreds of different banding materials. This includes not only varying colours but also tapes of different thicknesses in common dimensions of 2 mm, 1 mm, or even 0.5 mm. However, such a variety of materials and types can result in more frequent occurrences of incorrectly produced products.

Within the framework of the automation design and preparation of intelligent production in NADOP a.s. (Czech Republic), we focused on the automatic control of the edge banding process. Our work extends the edge banding error detection research from the publications (Chen, 2018), (Chen et al. 2022). The main task is to automatically check the glued edge, including edge type detection as well as edge banding error notification using artificial intelligence methods. Currently, the inspection in most enterprises is performed by the operator and there is poor or late detection of the problem. Published works (Aleksi, 2019; Wells, 2018) use neural networks to detect defects on wood such as edge knots, wane, split, pith, cracks, decays. This solution is currently very little published. The second important contribution of our work is the possibility of writing the inspection result directly into the product birth certificate and thus sharing real-time production information.

The proposed method for automated quality control of parts bonding comprises multiple stages. Initially, data was gathered via the OAK-D PoE camera to enable neural network training. This data was captured using the STEFANI EVOLUTION ONE taping machine. The camera and banding machine's specific parameters and configurations will be outlined in the Materials and Methods section. Image pre-processing is then conducted to improve the quality of the training image dataset. Using mathematical convolution operations, two types of filters, the Canny edge detector and Gabor filter, are applied to all of the images. Their theoretical background is described in detail in this paper, and the optimal settings are subsequently discussed in the Results section. These filters render the edges visible and accentuate any errors. In the second section, we present a personalised convolutional neural network. Additionally, we compare the effectiveness and precision of our proposed network in differentiating between six potential control states (various forms of error edges and different edge widths) against 11 pre-existing networks that have been modified.

Additionally, previous research solely examines operator-repairable defects and disregards defects needing multiple steps such as milling and edge re-gluing. Our solution encompasses these defects, thus expanding the practicality of its deployment. The suggested lapping inspection algorithms are universally applicable, facilitating their implementation in diverse production machine types.

MATERIAL AND METHODS

Description of the materials and used hardware

The following section concentrates on detailing the machines and hardware used to measure the experimental data, including the parameters. The entire production process takes place at NADOP a.s., Czech Republic.



Fig. 1: Banding machine STEFANI EVOLUTION ONE
Obr. 1: Olepovací stroj STEFANI EVOLUTION ONE

Figure 1 shows the STEFFANI EVOLUTION ONE banding and formatting machine on which the experimental measurements were carried out. It is an industrial banding machine suitable for medium-size industrial plants. It allows the continuous production of large quantities of parts for type 1 batch production. The machine is equipped with an industrial panel with MAESTRO PRO EDGE interface, with a high degree of automation, with the possibility of switching from a repetitive operation to several different processes sequentially, without the need for manual intervention in the banding process, in order to maximise the operator's time and production time. Our machine is equipped with a tray for 6 edges. The machine is ready for gluing with PUR and EVA adhesive, alternating as required.

The machine parameters include a part thickness range of 10-60 mm, edge thickness range of 0.3-3 mm, and a maximum feed speed of 40 m/min. For accurate measurement, the feed speed of the part on the conveyor is a crucial parameter. During experimental measurements, a continuous speed of 20 m/min was applied.

The machine satisfies Industry 4.0 standards as it can transmit the current production information to the information system. The machine is vertically integrated into the enterprise system with the aim of expanding the existing information framework in line with the Industry 4.0 initiative and the creation of a digital twin of the banding machine. Measured data is transmitted to the information system and stored with the part, while the product birth certificate is being extended.

The experimental data was obtained from 18mm DTD-L, a surface material composed of laminated chipboard with various colours and wood finishes.



Fig. 2: Camera OAK-D PoE producer Luxonis
Obr. 2: Kamera OAK-D PoE výrobcu Luxonis

The experimental measurement used a Luxonis colour camera, the OAK-D PoE model shown in Figure 2. The camera, which is IP67-rated and has an RJ46 Ethernet connector, is suitable for use in dusty environments such as the furniture industry. It is equipped with computer vision models that use neural networks, and its powerful processor allows it to run custom pre-trained neural network models. This architecture allows for a significant reduction in server or computer processing power, as the processing power is realised in the camera. The camera features stereophonic depth perception with filtering and post-processing, RGB depth alignment and high configurability for user applications.

Table 1 presents the parameters of the camera employed to measure the test data. A colour camera was utilised, placed behind the banding machine positioned over the roller conveyor, which facilitated the parts' return to the operator.

Table 1: Parameter OAK-D PoE
Tabuľka 1: Parametre Oak-D Poe

Camera Spec	Color camera	Stereo pair
Senzor	IMX378 (PY004 AF, PY052 FF)	OV9282 (PY003)
DFOV / HFOV / VFOV	81° / 69° / 55°	89° / 80° / 55°
Resolution	12MP (4056x3040)	1MP (1280x800)
Focus	AF: 8cm - ∞, FF: 50 cm - ∞	FF: 19.6 cm - ∞
Max Framerate	60 FPS	120 FPS
F-number	1.8 ±5%	2.0 ±5%
Lens size	1/2.3 inch	1/4 inch
Effective Focal Length	4.81mm	2.35mm
Distortion	< 1% AF, < 1.5% FF	< 1%
Pixel size	1.55µm x 1.55µm	3µm x 3µm
Dimension	130x101x31 mm	130x101x31 mm



Fig. 3: Camera OAK-D PoE installed on the machine
Obr. 3: Kamera OAK-D PoE inštalovaná na stroji

Figure 3 shows the camera mounted 52 cm above the roller conveyor behind the banding machine. At this height, the camera produces a recording in the default setting. The video is recorded at 8 frames per second. The individual frames of the video are processed by a neural network.

Image pre-processing

A high-quality camera is placed on the production belt, which continuously captures the glued edge. Our algorithm is able to process a real-time image of the scene and evaluate whether it is a correctly glued edge or an edge with some type of error described in the Introduction. However, the individual frames are affected by noise, so pre-processing is needed for quality processing (Mao et al. 2021). Also, instead of using images directly from the camera, it is advisable to use methods that highlight the differences between correctly and incorrectly glued edges.

We chose two types of filters, Canny (Canny 1986; Zhou et al. 2011) and Gabor filters (Gabor 1946; Mehrotra et al. 1992), as input images to the individual neural networks. We also tried edge detectors based on the first derivative (Sobel, Prewitt), second derivative (Laplace, Difference of Gaussian DoG), but their results did not sufficiently distinguish different types of errors from the correct edges. Comparison of these filters is in e.g. (Jain 2014).

In this section we describe the mathematical basis of the Canny edge detector and the Gabor filter. Both filters have convolution as their basis. Let $f(x,y)$ be an image matrix and let w be a filter of size $m \times n$. The convolution of the filter on the image can be written as:

$$w * f(x, y) = \sum_{s=-a}^a \sum_{t=-b}^b w(s, t) f(x - s, y - t) \quad (1)$$

Convolution is the process of transforming an image by applying a filter over each pixel and its local neighbours. It is a linear combination of the corresponding image pixel values and filter values (see Fig.4).

The values of the filter are chosen depending on what its task is. Averaging filters or Gaussian filters are suitable for removing additive noise in the image.

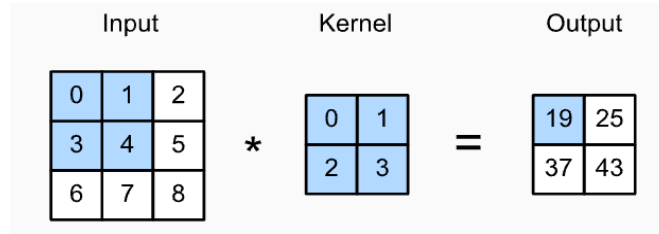


Fig. 4: Convolution - output blue pixel value is given by $0.0+1.1+3.2+4.3=19$
Obr. 4: Konvolúcia - výstupná hodnota modrého pixelu je daná $0.0+1.1+3.2+4.3=19$

Canny filter is an edge operator that uses a multi-step algorithm to detect strong edges in images. Canny filter consists of these four steps:

1. Apply a Gaussian filter to smooth the image in order to remove noise. Frequently, filter of size 5x5 is used:

$$\frac{1}{256} \begin{bmatrix} 1 & 4 & 6 & 4 & 1 \\ 4 & 16 & 24 & 16 & 4 \\ 6 & 24 & 36 & 24 & 6 \\ 4 & 16 & 24 & 16 & 4 \\ 1 & 4 & 6 & 4 & 1 \end{bmatrix} \quad (2)$$

Find the intensity gradients in the image:

$$grad(f) = [\partial f / \partial x \quad \partial f / \partial y] = [g_x, g_y] \quad (3)$$

and response of the filter is magnitude given by:

$$M(x, y) = \sqrt{g_x^2 + g_y^2} \quad (4)$$

2. Apply gradient magnitude thresholding to lower bound cut-off suppression to get rid of spurious response to edge detection.

3. Apply double threshold (high and low) to determine potential edges.

Second used filter is the Gabor filter, which is a Gaussian filter modulated by a plane wave. The convolution filter can be expressed as:

$$g(x, y; \lambda, \theta, \psi, \sigma, \gamma) = \exp\left(-\frac{x'^2 + \gamma^2 y'^2}{2\sigma^2}\right) \exp\left[i\left(2\pi\frac{x'}{\lambda} + \psi\right)\right] \quad (5)$$

where λ is wavelength of the plane wave, angle θ represents the orientation of the parallel stripes of the filter, σ is standard deviation, ψ is the phase of the plane wave, γ is the aspect ratio that defines the ellipticity of the function support.

$$x' = x \cos \theta + y \sin \theta, \quad y' = -x \sin \theta + y \cos \theta$$

In Fig. 5 is Gabor filter that is suitable for edge detection on wood panels. You can see that the shape is horizontal so that it is very effective for our edge shape detection. A detailed description of the filter and its application to individual images is given in the Results section.

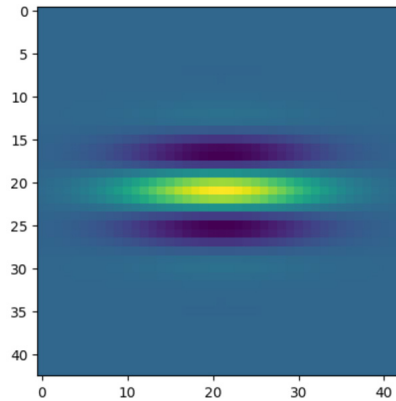


Fig. 5: Gabor filter visualisation.

Obr. 5: Gabor filter vizualizácia

Convolution neural network

The input images are modified using the previous filters (Canny, Gabor). We have developed several algorithms based on convolutional neural networks to recognise banding quality. The first tests were performed with our proposed neural network, described in the next section. We then modified 11 pre-trained neural networks to make them suitable for our inputs.

Today, neural networks are used in many areas of the furniture industry. They are used for quality control and production optimization. Their foundations were laid in the last century, but their development has only been possible in recent years, when the computing power of computers was sufficient to train complex models.

The basic idea comes from the study of how neurons work in the brain, where a neuron has multiple inputs and only one output. This gave rise to an element called a perceptron, which characterises the most basic unit of most neural networks.

Fig. 6 shows a schematic of a perceptron. It consists of inputs x_1, x_2, \dots, x_n , complemented by weights w_1, w_2, \dots, w_n . The input to the neuron consists of a linear combination of these values, to which we add a threshold, called bias b , to obtain the output.

The task of training a neural network is to optimally adjust the weights of the inputs. Each neuron also has an activation function. This determines whether the value of the linear combinations is sent on. The most commonly used are ReLU (Rectified Linear Unit), sigmoid or hyperbolic tangent. The advantage of these functions is that it is easy to calculate the derivative, which is necessary when learning a neural network during backpropagation. This area is theoretically challenging and not the focus of this paper, so we refer to the literature for further study (Jain et al. 2014).

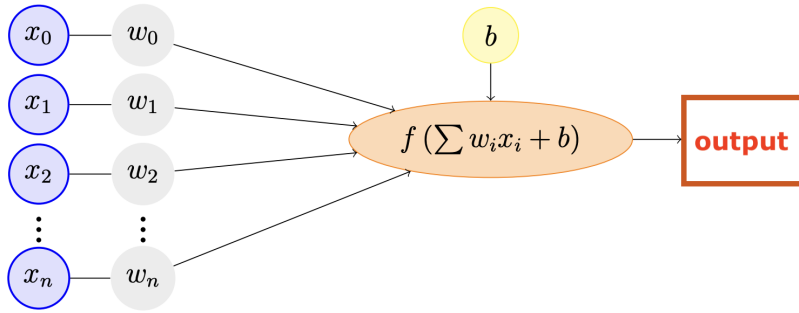


Fig. 6: The scheme of on perceptron

Obr. 6: Schéma perceptrónu

Creating a convolutional neural network is more complex. It is made up of many hidden layers, as working with each pixel would be computationally very demanding. In most cases, these layers are made up of a variety of convolutional kernels. The convolution operation is generally defined on continuous functions, but for use on images discrete convolution is used. We have described the general equation of convolution in the section describing filters as:

$$w * f(x, y) = \sum_{s=-a}^a \sum_{t=-b}^b w(s, t) f(x - s, y - t) \quad (6)$$

Convolution kernels can be specific, such as a Gaussian filter, an averaging filter for noise removal, or a Sobel operator for edge detection. In general, however, the values are chosen randomly in the CNN and corrected back during training to best discriminate the results between the input classes.

In addition, CNN is complemented by pooling, which reduces the size of the processed images and the computational complexity. For example, maximum pooling selects the largest element in a predefined image area (e.g. 2x2, 3x3). Thus, for a 3x3 pooling (corresponding to 9 pixels), the NN layer selects only one maximum value. This significantly reduces the size of the image and the computational complexity of the subsequent convolutional layers. Reducing the size of the images also allows important features to

be retained and improves CNN performance. Fig. 7 show the example of simple maximal pooling using 2x2.

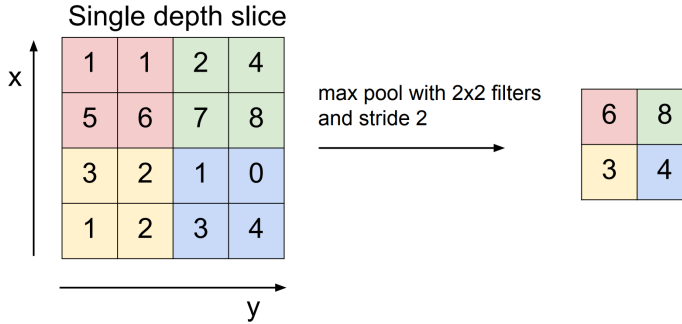


Fig. 7: Example of maximal pooling
Obr. 7: Príklad maximálneho poolingu

Batch normalisation layer is a neural network layer that is now commonly used in CNN. It helps to stabilise the network during training. Batch normalisation layer takes the outputs from the first hidden layer and normalises them before passing them on as the input of the next hidden layer. The normalisation means that we want zero mean and unit variance.

The last layer of CNN is usually the softmax layer. Softmax is an activation function that scales previous outputs into probabilities. The sum of these values will be equal to one, so we get the probability values for each class. The calculation is performed by the function $s: R^K \rightarrow [0,1]$, where $k \geq 1$. This function is defined for vector $z = (z_1, \dots, z_K)$ as:

$$s(z)_i = \frac{e^{z_i}}{\sum_{j=1}^K e^{z_j}} \quad (7)$$

For example, the standard softmax of a vector (6, 4, 9) is (0.047, 0.006, 0.946). This result means that the third class is the output with 94.6 percent of probability.

Our proposed CNN consists of ten hidden layers. The architecture consists of three convolutional layers, each using 10x10 filters. Each layer comprises eight of these filters. ReLU is employed as the activation function. Pooling is conducted by selecting the maximum pixel over a window size of 10x10. Batch Normalisation is added after each convolutional layer. The outputs are then vectorised using a flatten layer, with the output layer having six classes. These classes define the different banding situations that may arise. These classes define the different banding situations that may arise due to correctly glued edges at the start or end, as well as different types of poorly glued edges. The Python code of proposed CNN is:

```
model = Sequential([
    Conv2D(8, (10, 10), padding='same', activation='relu',
    input_shape=(299, 299, 3)),
```

```

        BatchNormalization(),
        MaxPooling2D(pool_size=(10, 10), strides=4),
        Conv2D(16, (10, 10), padding='same',
activation='relu'),
        BatchNormalization(),
        MaxPooling2D(pool_size=(10, 10), strides=4),
        Conv2D(32, (10, 10), padding='same',
activation='relu'),
        BatchNormalization(),
        Flatten(),
        Dense(6, activation='softmax')
])

```

To compare our solution, we have also created neural networks using eleven pre-trained networks (see Table 2 for detailed description). These convolutional neural networks are designed to recognize images from predetermined sets. For example, GoogLeNet has been trained on a million images and can classify 1,000 different categories. However, this is not necessary for our requirements. We can use the composition of the inner layers and train the CNN GoogLeNet with our data and outputs for the six classes related to the types of edges taped.

The advantage of these networks is their complexity. They are prepared by teams of experts and utilise different modern structures. E.. GoogLeNet structure for 1000 classes has 102,897,440 training parameters. Other networks likewise have counts of tens of millions. Our proposed CNN has merely 115,838 training values.

RESULTS

This chapter concentrates on presenting the outcomes and defining the parameters of the distinct parts. Initially, the deployment of the camera on the banding machine is elaborated. The input image received by the camera is then subjected to Canny and Gabor filters. Their exact parameters are illustrated in the figures and described here. Following this, we focus on neural networks. We compare our own proposed CNN, comprising only 115,838 parameters, with pre-trained neural networks containing one million training parameters. Our solution proves applicable for the edge bonding manufacturing process' automatic control.

Camera settings

To obtain training data, we connected a camera to a router and transferred the video to a PC. We subsequently extracted a series of images from the video as training data (images of 299x299x3 pixels). The resulting neural network was then transferred directly onto the camera for testing, enabling real-time evaluation of the given product image. The use of an AI-based camera speeds up the inspection process. During the experiment, the camera was positioned above the part passage point at a 52 cm height above the roller conveyor (see Fig. 3).

During the experimental measurements, our focus was on measuring the thickness of the edge and identifying various defects. These occurrences were divided into six classes

as input to the neural networks: absence of banding edge, 1 mm banding edge, 2 mm banding edge, start/end, long overlap of banding edge, and defect with a lack of ABS edge adhesion.

An advantage of our system proposal is its effortless expandability. If a new class arises, such as a varying edge thickness or a defect, additional training data can be incorporated to expand the current solution effortlessly.

Image filtering

As part of the initial preparation of the input edge images, it was necessary to enhance the edges and reduce noise. Two filters were implemented, namely the Canny edge detector and Gabor filter. The Canny edge detector was particularly user-friendly, requiring only a single value σ to be specified. Its optimal setting was determined empirically within the range of 0.1 to 5, using intervals of 0.1. The optimal value was found to be $\sigma = 1.2$. Fig. 8 illustrates a comparison of two different values for this parameter setting. We can observe that the double line edge is maintained for the optimal value.

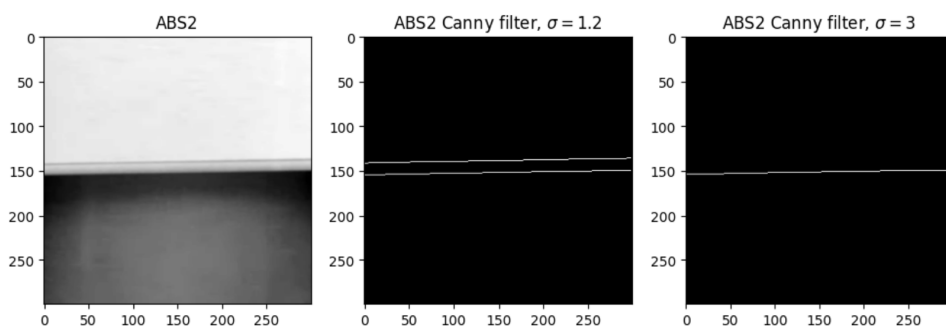


Fig. 8: Comparison of two Canny filters with different σ values for edge 2mm
Obr.8: Porovnanie dvoch Canny filtrov pre rôzne hodnoty parametra σ , hrana 2mm

For the Gabor filter, the parameters are less sensitive and with different settings we still get distinguishable sets of edge images with and without error. The crucial aspect to consider is selecting a rotation angle θ of 90 degrees because of the dominance of edge direction. Fig. 5 illustrates the used filter, and Fig. 9 reveals the application of this filter on a 2mm thick edge. To implement this in Python, use the following code:

```
ksize = 42
theta = np.pi/2
gabor_kern = cv2.getGaborKernel((ksize, ksize), 4.0, theta,
10.0, 0.5, 0,
ktype = cv2.CV_32F)
gabor_kern /= 1.5*gabor_kern.sum()
```

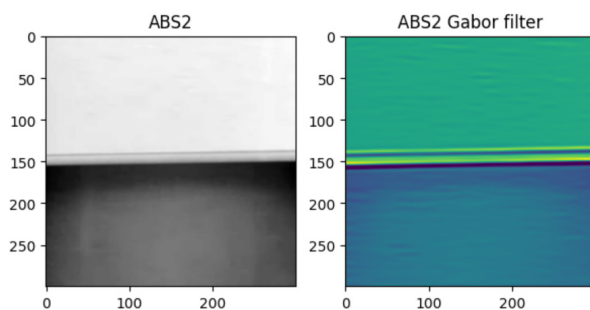


Fig. 9: Gabor filter - edge 2mm
Obr. 9: Filter Gabor - hrana 2mm

Proposed neural network

We developed a Python-based convolutional neural network using the Keras library. The objective was to create a network capable of detecting 6 classes. Fig. 10 displays the layers of our proposed convolutional neural network. The Convolutional Neural Network section provides a description and detailed explanation of each layer.

We utilised Matlab to adjust the pre-trained NNs due to its excellent user-friendliness and ability to accommodate many of the current neural networks. These pre-trained networks are capable of identifying user-defined image classes, including animals and plants. In our study, we repurposed their architecture and retrained them with our input categories while modifying the output to suit our requirements.

The following code presents a visualization of the alteration made to the final three layers of the CNN preceding the trained Googlenet. It illustrates the replacement of the layers, namely fc, softmax and class output.

```
numClasses = numel(categories(imdsTrain.Labels));
newLayers = [
    fullyConnectedLayer(numClasses,'Name','fc','WeightLearnRateFactor',10,'BiasLearnRateFactor',10)
    softmaxLayer('Name','softmax')
    classificationLayer('Name','classoutput')];
lgraph = addLayers(lgraph,newLayers);
```

To improve input data generalization, we employed data augmentation functions that rotated the images by angles ranging from -15 to 15 degrees, horizontally mirrored them, and shifted them on the vertical axis. The optimal displacement value, ranging from -30 to 30 pixels in the vertical direction, yielded the highest accuracy for the measured data. Data augmentation is an effective approach to training the neural network to handle unforeseen situations when only a limited number of training images are available.

Setting the training data-to-validation data ratio at 70:30 is also an important parameter for training neural networks. In order to ensure consistency, we trained various network models with the same settings for comparison purposes.

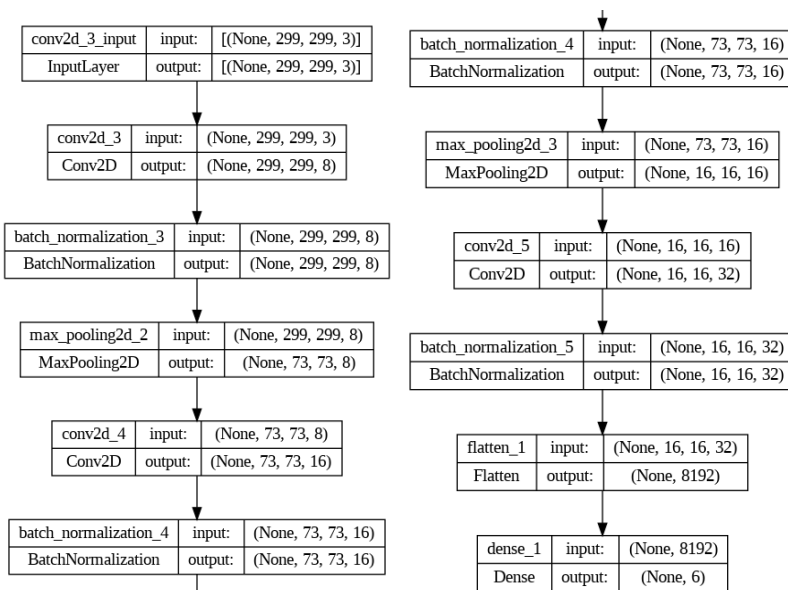


Fig. 10: Layers of proposed CNN
Obr. 10: Vrstvy navrhnutéj CNN

Table 2 displays the success rates of pre-trained neural network models on our measured data, using the Gabor filter and a learning rate of 0.001. All neural networks underwent a 3-epoch training process. Fig. 11 shows the training process for GoogleNet in Matlab environment and Fig. 12a then shows the training curve for the proposed CNN. We can see that at the end of the training process, the training curve is already stable and there is no significant improvement. This implies a good adjustment of the number of iterations and epochs.

In Table 2, it is evident that our proposed CNN achieves the highest success rate of 97.55 percent compared to the other networks. We trained our model using a higher number of iterations per epoch because we observed a continuous increase in accuracy from the progress of the training curve. In contrast, for the other pre-trained networks, increasing the number of iterations resulted in overtraining rather than an increase in accuracy. The proposed network's time consumption is comparable or superior. Nevertheless, in the case of the CNN, training time is not crucial since only the computed CNN coefficients are employed for evaluation.

Figure 12b illustrates the outcome of the CNN application on four randomly selected images (which were not part of the training or validation set), along with the corresponding probabilities. The application performs well, providing pertinent information regarding the edge type identification.

Table 2: Success rate of pre-trained neural networks with Gabor filter used
 Tabuľka 2: Úspešnosť predtrénovaných neurónových sietí s použitím Gabor filtra

Rank	Type of network	Success rate [%]	Iterations/epoch	Training time
0	Our CNN	97,55	35	1:32:20
1	Resnet101	93,33	26	0:40:09
2	Googlenet	91,94	25	0:10:21
3	Densenet201	91,41	26	0:55:55
4	Resnet50	91,16	25	0:22:41
5	Nasnetlarge	89,3	25	7:49:57
6	Darknet53	89,04	26	0:46:16
7	Xception	87,85	26	1:05:28
8	Vgg16	86,82	25	0:44:19
9	Nasnetmobile	84,5	25	0:23:19

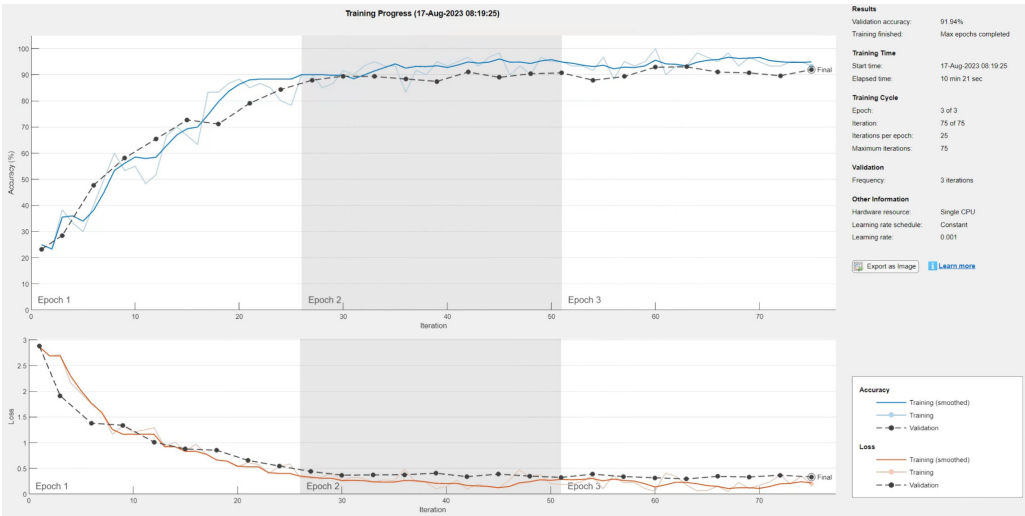


Fig. 11: Googlenet training progress
 Obr. 11: Googlenet priebeh tréningu

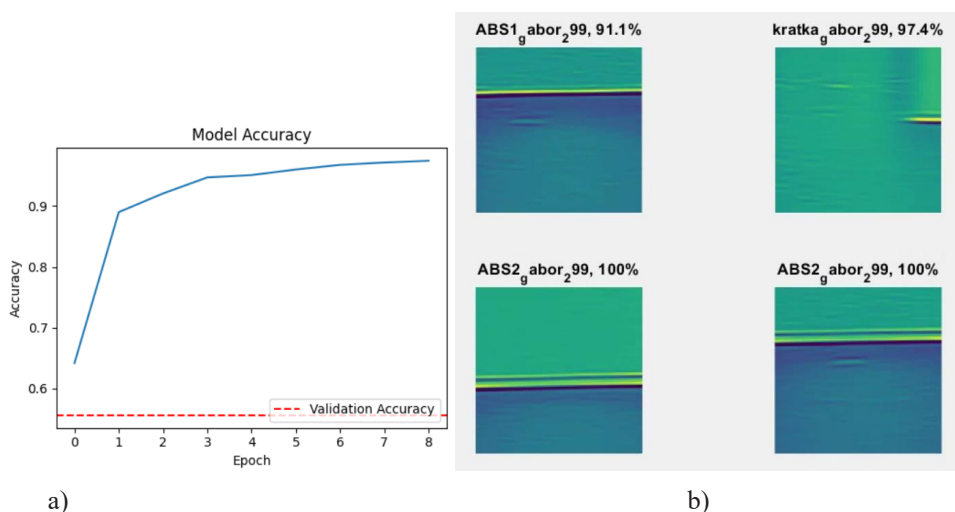


Fig. 12: a) CNN's own training progress, b) Gabor filter results - edge 2mm,
Obr. 12: a) Priebeh trérovania vlastnej CNN, b) Filter Gabor výsledky - hrana 2mm

DISCUSSION AND CONCLUSION

The work focuses on automatic inspection of the banded edge on a banding machine using an AI-enabled camera that processes the image. The proposed method for image filtering is Gabor and Canny. Subsequently, neural network models were compared for automatic recognition, and our proposal was found to surpass the previously trained models in several aspects for utilization in Edge AI.

Our neural network (comprising of 118,000 training parameters) outperforms previously developed models. Compared to pre-trained models with tens of millions of training parameters, our network is more memory-efficient and easier to implement on Edge AI devices.

The outcome suggests a proposal for furniture manufacturers and upgrades to their current banding machines, meeting Industry 4.0 specifications, at a moderate expense. The measurements were executed with AI-integrated, robust hardware suitable for actual production line settings. This proposal alleviates the stress on the organization's network architecture, as the camera carries out all computations. The identified data from the camera is prepared to be transmitted through the network to the superior system and recorded in the product's birth certificate. Afterward, this data will be examined within the automated production cells to ensure that the applied edge banding is appropriately applied.

ACKNOWLEDGMENT

MPO: 283268/21/61200/351, CZ.01.1.02/0.0/0.0/20_324/0023587, Pilotní vývoj základů funkcí digitálního dvojčete pro zlepšení výrobních procesů ve firmě NADOP

REFERENCES

- AKANSHA, J., MUKESH, G., SATYANARAYAN, T., DEPIKA, 2014. Comparison of edge detectors. s. 289-294. 10.1109/MedCom.2014.7006020.
- ALEKSI, I., SUŠAČ, F., MATIĆ, T., 2019. Features extraction and texture defect detection of sawn wooden board images. In: 2019 27th Telecommunications Forum (TELFOR), IEEE, pp 1–4
- CANNY, J., 1986, A Computational Approach To Edge Detection. Pattern Analysis and Machine Intelligence, IEEE Transactions on. PAMI-8. s. 679 - 698. 10.1109/TPAMI.1986.4767851.
- ČERVENÝ, L., SLOUP, R., ČERVENÁ, T., 2022. The Potential of Smart Factories and Innovative Industry 4.0 Technologies-A Case Study of Different-Sized Companies in the Furniture Industry in Central Europe. Forests. 13. 2171. 10.3390/f13122171.
- ČERVENÝ, L., SLOUP, R., ČERVENÁ, T., RIEDL, M., PALÁTOVÁ, P., 2022. Industry 4.0 as an Opportunity and Challenge for the Furniture Industry—A Case Study. Sustainability, 14, 13325. <https://doi.org/10.3390/su142013325>
- CHEN, N., MEN, X., HAN, X., WANG, X., SUN, J., 2018. Edge detection based on machine vision applying to laminated wood edge cutting process. In: 2018 13th IEEE conference on industrial electronics and applications (ICIEA), IEEE, pp 449–454
- CZIMMERMANN, T., CIUTL, G., MILAZZO, M., CHIURAZZI, M., ROCCELLA, S., ODDO, C., DARIO, P., 2020. Visualbased defect detection and classification approaches for industrial applications-a survey. Sensors r. 20(5):1459
- GABOR, D., 1946. Theory of communication. J. Inst. Electr. Eng. 93
- JAIN, A., GUPTA, M., 2014. S. N. Tazi and Deepika, "Comparison of edge detectors," International Conference on Medical Imaging, m-Health and Emerging Communication
- MAO, J., WU, Z., FENG, X., 2021. Image Definition Evaluations on Denoised and Sharpened Wood Grain Images. Coatings, 11, 976. <https://doi.org/10.3390/coatings11080976>
- MEHROTRA, R., NAMUDURI, K.R., RANGANATHAN, N., 1992. Gabor filter-based edge detection, Pattern Recognition, Volume 25, Issue 12, 1479-1494, ISSN 0031-3203, [https://doi.org/10.1016/0031-3203\(92\)90121-X](https://doi.org/10.1016/0031-3203(92)90121-X).
- WANG, L., HE, J., XU, S., 2017. The Application of Industry 4.0 in Customized Furniture Manufacturing Industry. MATEC Web of Conferences. s. 100. 03022. 10.1051/mateconf/201710003022.
- WELLS, L., GAZO, R., DEL, R.R., KRS, V. BENES, B., 2018. Defect detection performance of automated hardwood lumber grading system. Comput Electron Agric, 155:487–495
- ZHOU, P., YE, W.W., WANG, Q., 2011. An Improved Canny Algorithm for Edge Detection. Journal of Computational Information Systems, 7(5), s. 1516-1523.

Corresponding author:

Name Surname: Bronislav Dřimal, tel.: +420773928027, e-mail: bronislavdřimal@email.cz